

# Lagrangian Eddy Trapping Fosters Chlorophyll Hot Spots in the North Pacific Subtropical Gyre

Alexandra Elizabeth Jones-Kellett<sup>1</sup> and Michael J. Follows<sup>2</sup>

<sup>1</sup>Massachusetts Institute of Technology

<sup>2</sup>MIT

December 3, 2023

## Abstract

Vertical motions associated with mesoscale ocean eddies modulate the light and nutrient environment, stimulating anomalies in phytoplankton biomass and chlorophyll. Phytoplankton populations can be subsequently trapped by the horizontal circulation or laterally diluted. In a time-varying flow, Lagrangian methods can be used to quantify eddy trapping, also known as Lagrangian coherency. From two decades of remote sensing observations in the North Pacific Subtropical Gyre, we compared coincident Eulerian and Lagrangian eddy atlases to assess the impact of eddy trapping on chlorophyll concentration. We found higher chlorophyll within Lagrangian coherent boundaries than in Eulerian eddies and outside-eddy waters. Yet, there are differences regionally and seasonally. For example, chlorophyll is most enriched within coherent boundaries of the Hawaiian Lee eddies and to the south of 23N in fall and winter. Our results suggest that by not accounting for lateral dilution, Eulerian analyses may underestimate the role of mesoscale eddies in enhancing chlorophyll.

# Lagrangian Eddy Trapping Fosters Chlorophyll Hot Spots in the North Pacific Subtropical Gyre

Alexandra E. Jones-Kellett<sup>1,2</sup>, Michael J. Follows<sup>1</sup>

<sup>1</sup>Department of Earth, Atmospheric, and Planetary Sciences, Massachusetts Institute of Technology,  
Cambridge, MA, USA

<sup>2</sup>Biology Department, Woods Hole Oceanographic Institution, Woods Hole, MA, USA

## Key Points:

- Cumulatively, Lagrangian coherent eddies have anomalously high surface chlorophyll relative to dispersive eddies and outside-eddy waters.
- The biological response to eddy trapping differs regionally, seasonally, by eddy age, and polarity.
- Coherent Hawaiian Lee eddies have the most extreme chlorophyll anomalies year-round relative to outside-eddy waters.

---

Corresponding author: Alexandra E. Jones-Kellett, [jonesae@mit.edu](mailto:jonesae@mit.edu)

**Abstract**

Vertical motions associated with mesoscale ocean eddies modulate the light and nutrient environment, stimulating anomalies in phytoplankton biomass and chlorophyll. Phytoplankton populations can be subsequently trapped by the horizontal circulation or laterally diluted. In a time-varying flow, Lagrangian methods can be used to quantify eddy trapping, also known as Lagrangian coherency. From two decades of remote sensing observations in the North Pacific Subtropical Gyre, we compared coincident Eulerian and Lagrangian eddy atlases to assess the impact of eddy trapping on chlorophyll concentration. We found higher chlorophyll within Lagrangian coherent boundaries than in Eulerian eddies and outside-eddy waters. Yet, there are differences regionally and seasonally. For example, chlorophyll is most enriched within coherent boundaries of the Hawaiian Lee eddies and to the south of 23°N in fall and winter. Our results suggest that by not accounting for lateral dilution, Eulerian analyses may underestimate the role of mesoscale eddies in enhancing chlorophyll.

**Plain Language Summary**

Eddies are ubiquitous rotating ocean currents up to hundreds of kilometers in diameter. While some eddies continuously mix with their surroundings, others trap their constituents that do not escape until the eddy dissolves. We refer to the former eddy behavior categorically as leaky or dispersive, while the latter is coherency. Phytoplankton are microscopic, free-floating microbes subject to the whims of ocean currents, including eddies. They contain the pigment chlorophyll within their cells that allows them to photosynthesize and subsequently alter the color of the ocean. In this study, we used satellite datasets and simulations of currents in the North Pacific to examine the effect of eddy coherency on local concentrations of phytoplankton, estimated by the greenness of the surface ocean. We found little difference in chlorophyll concentration in leaky and coherent eddies north of the Hawaiian Islands. To the south, we observed significantly greener waters in coherent eddies than in their leaky counterparts in the winter and fall. We suggest that, in some regions, studies may underestimate the role of leaky eddies in stimulating plankton blooms if they are quickly mixed with surrounding waters, which has implications for the ocean carbon budget.

**1 Introduction**

The North Pacific Subtropical Gyre (NPSG) has low phytoplankton biomass but is subject to high ecosystem variability (Karl & Church, 2017). Mesoscale eddies contribute to this variability, bringing nutrient-rich deep waters to the oligotrophic surface of the gyre via eddy-wind interactions and eddy pumping that stimulates phytoplankton growth (McGillicuddy Jr, 2016). Eddies in the NPSG including Station ALOHA and the Hawaiian Lee eddies are the focus of seminal works capturing biophysical interactions. For example, observations reveal that eddies affect biogeochemical cycling by enhancing primary production (Falkowski et al., 1991; Allen et al., 1996; Nicholson et al., 2008), altering phytoplankton community structure (Olaizola et al., 1993; Vaillancourt et al., 2003; Brown et al., 2008; Fong et al., 2008; Barone et al., 2019; Harke et al., 2021), and intensifying carbon export (Bidigare et al., 2003; Benitez-Nelson et al., 2007; Rii et al., 2008; Zhou et al., 2021). The NPSG is Earth’s largest ecosystem, thus the integrated effects of mesoscale biophysical interactions therein may play a significant role in the global carbon cycle.

Ocean eddies also influence the horizontal advection of phytoplankton, potentially acting to isolate communities (Provenzale, 1999) and preserve them across ocean basins (Lehahn et al., 2011; Villar et al., 2015). Further, lateral trapping can modulate trophic interactions (d’Ovidio et al., 2013) and generate plankton patchiness by localizing blooms (Gower et al., 1980; Fennel, 2001). In this study, we refer to eddies that trap for months

or longer as “coherent”. Mesoscale eddies that are detected from the Sea Level Anomaly (SLA) by assuming geostrophic balance (Chelton, Schlax, & Samelson, 2011; Chelton, Gaube, et al., 2011) are not necessarily coherent through time (Beron-Vera et al., 2013; Wang et al., 2015). To accurately measure eddy coherency in a time-varying flow, a Lagrangian perspective is needed (Haller, 2015). Interpreting biophysical interactions from a Lagrangian perspective naturally follows since phytoplankton experience a moving frame of reference (Woods & Onken, 1982; Lehahn et al., 2018).

Satellite remote sensing of SLA and chlorophyll-*a* (chl-*a*; a proxy for phytoplankton biomass) reveals significant relationships between ocean color anomalies and mesoscale eddies in subtropical waters (Gaube et al., 2014; Dufois et al., 2016; He et al., 2016; Huang et al., 2017; Xu et al., 2019; Travis & Qiu, 2020). However, these studies employ Eulerian methods and cannot determine the contribution of eddy trapping toward altering chl-*a* concentrations. By comparing complementary Lagrangian and Eulerian eddy atlases, we tested the hypothesis that the waters within coherent vortices more effectively maintain anomalous chl-*a* concentrations than leaky eddies (Figure S1). This is illustrated by the following idealized model that describes surface chl-*a* concentration in an eddy ( $B_{in}$ ):

$$\frac{dB_{in}}{dt} = \mu B_{in} - \Psi(B_{in} - B_{out}). \quad (1)$$

Here  $B_{out}$  is the outside-eddy concentration,  $\mu$  is the biological rate of change (e.g., growth, mortality, photoacclimation) in the eddy, and  $\Psi$  is the lateral fluid exchange rate at the eddy boundary. Chl-*a* concentrations increase inside an eddy when  $\mu B_{in} > \Psi(B_{in} - B_{out})$ . A coherent eddy minimizes  $\Psi$  over the timescale of interest. Thus,  $\frac{dB_{in}}{dt}$  will be greater in a coherent eddy than in a dispersive eddy with the same  $\mu$  and  $B_{out}$ , resulting in relatively higher chl-*a*. Our analysis of two decades of satellite data in the NPSG indeed reveals “hot spots” of chlorophyll (Calil & Richards, 2010) in Lagrangian coherent eddies and we uncover regional and seasonal differences in the biological signature of eddy trapping.

## 2 Materials and Methods

The domain includes 2000-2019 and the region 15-30°N, 180-230°. The spatial bounds reduce the degrees of freedom introduced by large-scale environmental variability from the ultra-oligotrophic western NPSG, Transition Zone Chlorophyll Front (Glover et al., 1994), California Current System, and equatorial currents (Figure S2). Moreover, focusing on a small area afforded a comprehensive evaluation of sub-regional and seasonal patterns. We used CMEMS 1/4° daily satellite geostrophic current and SLA data for eddy identification. 8-day average satellite chl-*a* data were obtained from OC-CCI with a spatial resolution of 4km at the equator (Sathyendranath et al., 2019).

### 2.1 Eddy Atlases

We used the OceanEddies software to generate an Eulerian eddy atlas from daily SLA (Faghmous et al., 2015). The algorithm identifies an eddy boundary as the outermost closed contour containing a single SLA extremum and tracks features through time. We required eddies to have a minimum lifetime of 32 days and contain at least twelve 1/4° grid cells. The smallest SLA eddy has an area of 8,048km<sup>2</sup> with a radius  $\approx 50$ km, consistent with the Rossby radius of deformation in the region of interest (Chelton et al., 1998). We set the eddy disappearance parameter to 3 days to account for noise in the data and prevent prematurely “killing” an eddy. We reduced the temporal resolution of the SLA atlas to an 8-day frequency for the ensuing analysis. In total, we tracked 6,846 SLA eddies (52,553 polygons), including 3,322 anticyclones characterized by SLA maxima and 3,524 cyclones by SLA minima.

Haller et al. (2016) introduced the Lagrangian Averaged Vorticity Deviation (LAVD), a measure of the integrated vorticity of a Lagrangian particle over a timescale of interest. An LAVD field is produced by mapping the LAVD for a grid of Lagrangian particles at their initialization locations. A fluid set in rigid-body rotation is identified as a closed contour surrounding a local maximum in the LAVD field, referred to as a Rotationally Coherent Lagrangian Vortex (RCLV) (Haller et al., 2016; Tarshish et al., 2018). Specifically tailored to biogeochemical applications, Jones-Kellett and Follows (*in review*, 2023) identified and tracked 32-day RCLVs in the NPSG at an 8-day resolution using backward-in-time particle simulations synchronized with the OC-CCI 8-day chl-*a* product (Figure S3). The atlas follows RCLVs from age 32 days and onward. Here, we expanded the dataset to capture RCLV genesis because young eddies are associated with biological anomalies (Gaube et al., 2013). To do so, we initialized Lagrangian particles in 32-day-old RCLVs and tracked them backward-in-time with the OceanParcels software (Delandmeter & van Sebille, 2019). At each 8-day “timestep” (ages 24, 16, and 8), we drew closed contours to encompass the particle set (Figure S4). The atlas contains 11,855 tracked RCLVs (75,445 polygons), including 5,592 anticyclones characterized by a negative sign of relative vorticity and 6,263 cyclones by a positive sign.

## 2.2 Chlorophyll Anomalies

We categorized each pixel from the satellite chl-*a* fields as background (i.e., outside-eddy) or inside an eddy. Some, though not all SLA eddies overlap with an RCLV, and vice versa. Thus, the in-eddy pixels are within an SLA eddy, RCLV, or both. We refer to the pixels inside an SLA eddy boundary but not an RCLV as “SLA excluding RCLV” (Figure S5). This includes the most dispersive regions of the eddy. The “SLA eddy” category includes all pixels within the eddy boundaries irrespective of whether it contains an RCLV.

The climatological chl-*a* anomaly is a temporal metric defined

$$\delta c_{clim}(x, y, t) = c(x, y, t) - \frac{1}{M} \sum_{t'=0}^M c(x, y, t') \quad (2)$$

where  $c(x, y, t)$  is the chl-*a* at location  $(x, y)$  and time  $t$ .  $\frac{1}{M} \sum_{t'=0}^M c(x, y, t')$  describes the 2000-2019 mean chl-*a* in the month corresponding to the date  $t$  (i.e., the monthly climatology; Figure S6). A positive  $\delta c_{clim}$  indicates that chl-*a* is higher than average for that location and month. We used  $\delta c_{clim}$  to identify changes in chl-*a* related to the mesoscale activity that were distinct from the seasonal cycle.

We define the relative difference in the eddy and background probability density distributions (PDD) of  $\delta c_{clim}$  as

$$f(\delta c_{clim}) = \frac{p_E(\delta c_{clim}) - p_B(\delta c_{clim})}{p_B(\delta c_{clim})} \quad (3)$$

where  $p_E(\delta c_{clim})$  is the PDD of the climatological chl-*a* anomalies in an eddy type and  $p_B(\delta c_{clim})$  is the PDD of anomalies in the background ocean.  $f(\delta c_{clim})$  is interpreted as the likelihood of observing a given chlorophyll anomaly in the eddy type compared to the background. For example,  $f(\delta c_{clim}) > 0$  means the value of  $\delta c_{clim}$  is more likely to be observed in an eddy than outside an eddy.

The local chl-*a* anomaly is a spatial metric defined

$$\delta c_{loc} = \frac{1}{A_{in}} \oint_I c(x, y) dI - \frac{1}{A_{out}} \oint_O c(x, y) dO. \quad (4)$$

$I$  is the eddy polygon with area  $A_{in}$  and  $O$  is the “donut” polygon from the eddy boundary to double the eddy radius with area  $A_{out}$ . Thus,  $\frac{1}{A_{in}} \oint_I c(x, y) dI$  is the average chl-*a* inside the eddy, and  $\frac{1}{A_{out}} \oint_O c(x, y) dO$  is the average in the immediate surroundings

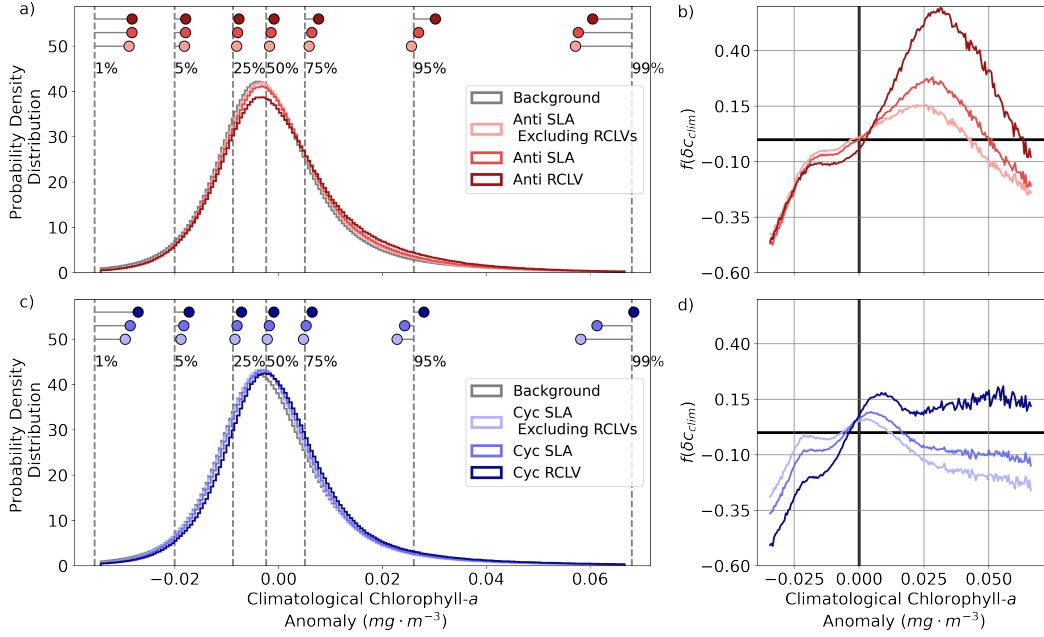


**Figure 1.** Probability density distributions (PDD) of the climatological chl-*a* anomalies ( $\delta c_{clim}$ ; Equation 2) in (a) anticyclones and (c) cyclones from the 1 – 99% quantiles. The dotted gray lines depict the quantiles of the background distribution, and the dots show the equivalent quantiles for each eddy category.  $f(\delta c_{clim})$  is the relative difference in the eddy PDD from the background PDD (Equation 3) for (b) anticyclones and (d) cyclones.

of the eddy. A positive  $\delta c_{loc}$  indicates that the mean chl-*a* concentration in the eddy is higher than surrounding waters.

### 3 Results

We address the hypothesis that coherent, isolated eddies will maintain anomalous chl-*a* longer than their dispersive counterparts. First, we address the cumulative impacts of eddy trapping. Next, we examine seasonal and sub-regional differences in the biological signature of eddy coherency.

#### 3.1 Cumulative Effect of Eddy Trapping

Cumulatively, surface chl-*a* is higher per unit area in RCLVs than in SLA eddies for both polarities (Table S1). On average, there is more surface chl-*a* in anticyclones than in the background and less in cyclones. Figure 1 shows the probability density distributions of the chl-*a* anomaly relative to the local, seasonal climatology ( $\delta c_{clim}$ ; Equation 2) for anticyclones (a) and cyclones (c). The quantiles of the distributions (indicated by the dots) show a consistent shift toward anomalously high chl-*a* in RCLVs (Figure 1a,c). An exception is the 99% quantile for anticyclones, which is lower than the background. This indicates that positive anomalies are more likely to occur in anticyclonic eddies than in the background ( $f > 0$ ; Equation 3) except at extremely high  $\delta c_{clim}$  (Figure 1b). Coherent cyclones have  $f > 0$  for all positive  $\delta c_{clim}$  (Figure 1d). Conversely, cyclonic SLA eddies have positive anomalies less frequently. 21% of chl-*a* in anticyclonic SLA eddies (Table S2) and 23% in cyclonic SLA eddies (Table S3) are also contained within an RCLV. We isolate the leakiest eddy zones when excluding RCLV-associated contri-

butions (“SLA excluding RCLVs” in Figure 1). Fewer positive chl-*a* anomalies are attributed to these zones in both polarities. Eddies are less likely than the background to have negative chl-*a* except for low-magnitude anomalies in cyclones.

### 3.2 Regional and Seasonal Subdomains

We examined the distributions of  $\delta c_{clim}$  seasonally and regionally to explore variations in how eddy trapping shapes chl-*a* in the NPSG. We determined mesoscale-driven subdomains by the eddy polarity probability ( $P$ ) (Chaigneau et al., 2009), defined

$$P(x, y) = \frac{F_A(x, y) - F_C(x, y)}{F_A(x, y) + F_C(x, y)}. \quad (5)$$

$F_A(x, y)$  ( $F_C(x, y)$ ) is the number of times the pixel at location  $(x, y)$  was inside an anticyclone (cyclone) from 2000-2019. Anticyclonic eddy polarity is more frequent than cyclonic when  $P > 0$ . Figure 2a depicts the geographic distribution of  $P$  for RCLVs, revealing more anticyclonic activity north of 23°N, cyclonic domination to the southeast of Hawai‘i, and Lee eddy signatures to the west.

There are distinctive chl-*a* signatures between northern and southeastern eddies (Figure 2). In the north, cyclones are less likely than the background to have positive  $\delta c_{clim}$  in all seasons except the summer. Northern cyclones are more likely to have a negative  $\delta c_{clim}$  than the background in winter and fall when domain-average chl-*a* concentrations are at the annual maximum (Figure S6, S7). According to Equation 1, a decrease in chl-*a* concentration ( $B_{in}$ ) may occur when  $\mu B_{in} < \Psi(B_{in} - B_{out})$ . In an RCLV where  $\Psi$  is minimized, it is likely that a low population growth rate,  $\mu$ , results in lower chl-*a*. For example, low nutrient supply rates may decrease growth rates, mortality may increase, or the cellular chlorophyll-to-carbon ratio can decrease due to increased light availability (Geider, 1987; MacIntyre et al., 2000). Northern anticyclones exhibit nearly opposite signatures than cyclones, with  $f > 0$  for positive  $\delta c_{clim}$  (except for extreme anomalies) in fall and winter. Anticyclonic RCLVs (and not SLA eddies) are likelier to have a negative chl-*a* anomaly relative to the summer and fall background. Leaky anticyclones uniquely have  $f > 0$  for highly positive  $\delta c_{clim}$  in the summer when mixing with surrounding chl-*a* elevated waters (high  $\Psi$  and high  $B_{out}$ ) may increase concentrations inside SLA anticyclones.

In the southeast province, the distributions of  $\delta c_{clim}$  in cyclones are inordinately different from that of the north. All types of cyclones have  $f < 0$  for negative  $\delta c_{clim}$  year-round, suggesting cyclones in this region enhance chl-*a*. In the fall and winter, cyclonic RCLVs are likelier to have a positive  $\delta c_{clim}$  than the background and SLA eddies. Because the chl-*a* signatures of cyclonic SLA eddies excluding RCLVs are like the background, positive anomalies in cyclonic SLA eddies are mostly contained within nested RCLVs. Thus, eddy trapping plays a significant role in the elevated chl-*a* in cyclones of the southeast province. Anticyclones in the southeast have  $f > 0$  for low magnitude positive  $\delta c_{clim}$  in the winter and spring. The distributions of  $\delta c_{clim}$  differ between RCLVs and SLA anticyclones during these seasons, suggesting that eddy trapping plays a distinctive role. Anticyclones are more likely than the background to host negative  $\delta c_{clim}$  in the fall. Anticyclones are less prevalent in the southeast province, so these observations play a small role in the cumulative effect in the gyre.

In summary, there are latitudinal biophysical differences within the NPSG. Anticyclones have high chl-*a* anomalies in the north during fall and winter and eddy trapping plays a minimal role in altering chl-*a* concentrations. In the southeast, cyclones foster high chl-*a* in fall and winter and chl-*a* is significantly higher in Lagrangian coherent vortices than in Eulerian eddies.

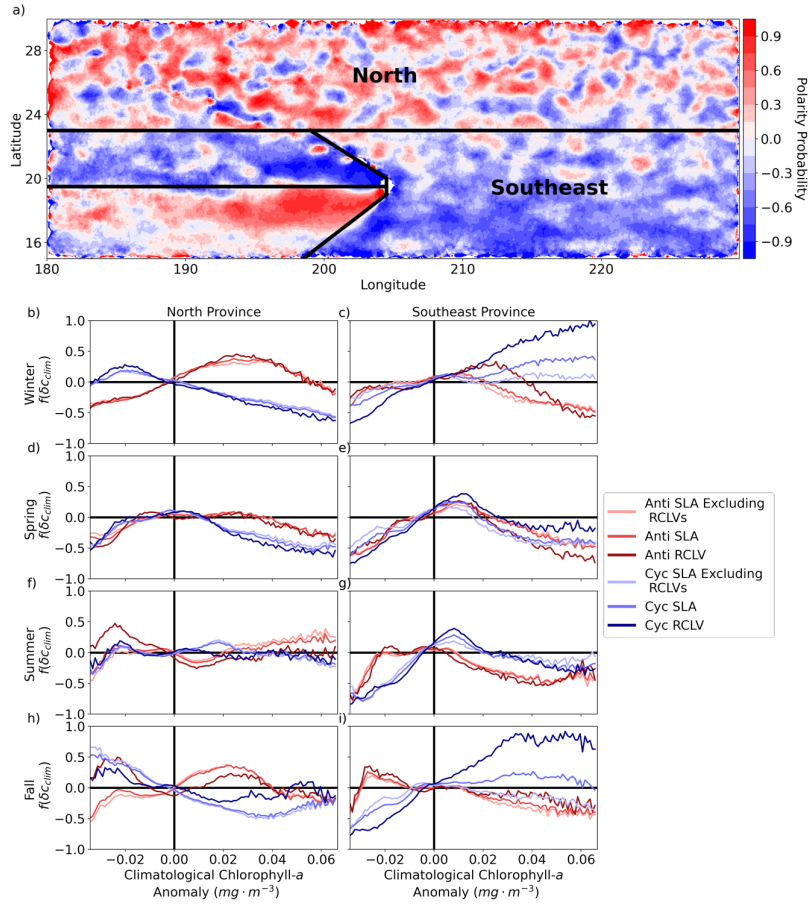


**Figure 2.** (a) RCLV polarity probability. Red (blue) indicates that anticyclones (cyclones) are more common at the location. The black lines delineate mesoscale-driven provinces. (b-i) The relative difference in the probability density distribution of the climatological chl-*a* anomaly from the background ( $f(\delta_{C_{lim}})$ ) for each eddy type. Each row corresponds with a season (winter includes December to February). Figures S8 and S9 show the underlying probability density distributions.

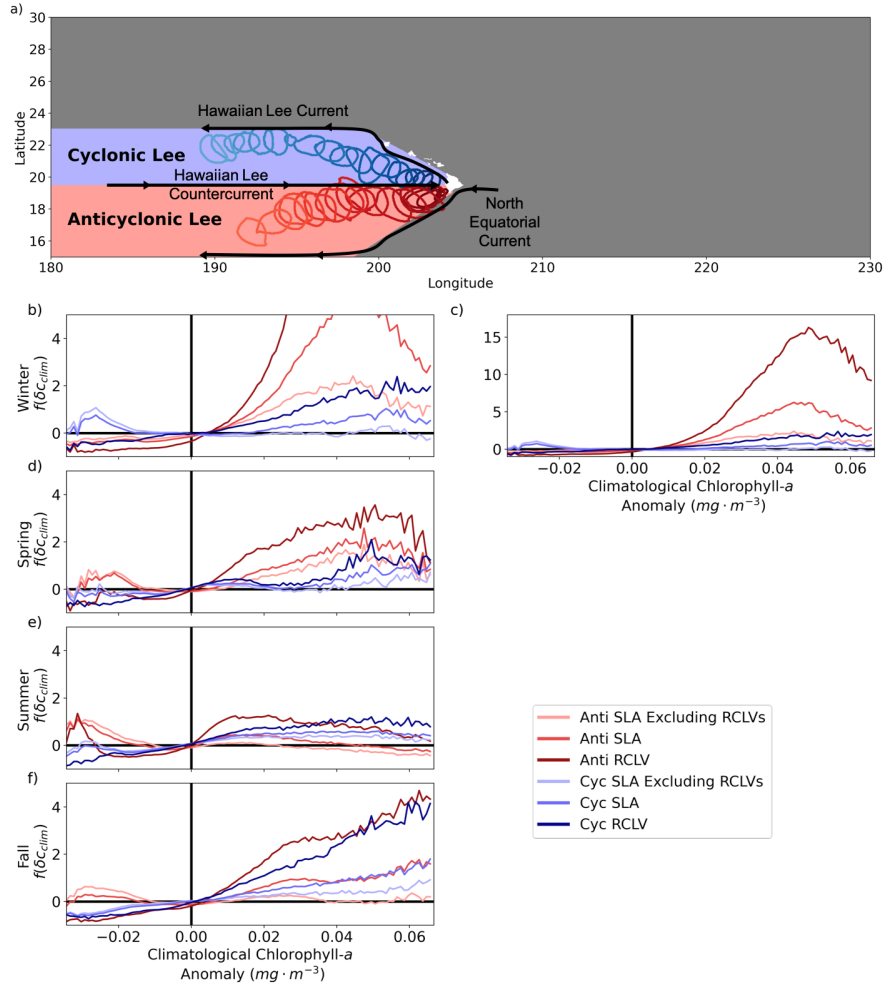


**Figure 3.** (a) Schematic of the currents that sustain the Hawaiian Lee eddies. The region dominated by cyclones (anticyclones) is blue (red). Two RCLV boundaries plotted every 16 days show the common propagation pathways westward from the islands. (b-f) The relative difference in probability density distributions of the climatological chl-*a* anomaly from the background ( $f(\delta c_{clim})$ ). Note that the y-axis differs from Figure 2 to accommodate larger values. Figure S10 depicts the underlying probability density distributions. Panel (c) includes the same information as (b) with a different y-axis to expose the curves.

### 3.3 Hawaiian Lee Eddies

The ‘‘Hawaiian Lee eddies’’ are large, long-lived features formed in the Lee of the Hawaiian Islands (Figure 3a). The shear instability between the eastward-flowing Hawaiian Lee Countercurrent and the westward-flowing North Equatorial Current generates anticyclones (Calil et al., 2008; Yoshida et al., 2010; Y. Liu et al., 2012). A wind stress curl anomaly associated with blocking trade winds by the islands produces cyclones (Lumpkin, 1998; Yoshida et al., 2010). The Hawaiian Lee Countercurrent to the south and the westward-flowing Hawaiian Lee Current to the north sustain the cyclonic vorticity.

RCLVs and SLA eddies of both polarities have  $f > 0$  for positive  $\delta c_{clim}$  year-round (Figure 3b-f). Trapping also plays a significant role in the chl-*a* signature of the Hawaiian Lee eddies. RCLVs have more positive chl-*a* anomalies than SLA eddies and the background ocean. We found a similar chl-*a* response to cyclonic and anticyclonic RCLVs in the summer and fall. However, anticyclones are more likely to have positive anomalies than cyclones in the winter and spring. Even the leakiest anticyclonic features (i.e., SLA excluding RCLVs) host positive  $\delta c_{clim}$  during these seasons. In the winter, anticyclonic RCLVs can be up to 15 times more likely than the background to have a positive  $\delta c_{clim}$ , whereas cyclonic RCLVs are up to 2 times as likely.

### 3.4 Chlorophyll Evolution of Long-lived Eddies

The Lagrangian eddy atlas enables the examination of chl-*a* patches as they evolve through time in quasi-isolated systems. Accordingly, we analyzed the in-eddy chl-*a* anomaly compared to the immediate surroundings,  $\delta c_{loc}$  (Equation 4), as a function of age for 245 RCLVs (109 anticyclones, 136 cyclones; Figure 4) that maintained coherency for 150 or more days. Figure S11 illustrates the westward propagation of these features. The magnitudes of  $\delta c_{loc}$  complement the results of Sections 3.2 and 3.3. For example, RCLVs in the north minimally alter chl-*a* compared to their surroundings except for wintertime anticyclones. In that case, the largest anomalies occur early in the lifetime. Cyclonic RCLVs foster heightened chl-*a* that declines with eddy age in the winter and fall in the southeast. Hawaiian Lee RCLVs dramatically localize chl-*a*, and this is the only domain where RCLVs have increasing  $\delta c_{loc}$  with eddy age. The results show that there is not a uniform slope of change in chl-*a* as a function of eddy age. Rather, chl-*a* evolves in coherent eddies depending on the region, season, and eddy polarity.

We apply the model of chl-*a* concentrations in eddies (Equation 1) to interpret the rate of change in  $\delta c_{loc}$  with RCLV age such that

$$\frac{d}{dt}(\delta c_{loc}) = \frac{dB_{in}}{dt} - \frac{dB_{out}}{dt}. \quad (6)$$

Consider the case where  $\mu$  is equivalent in and out of the eddy. This is likeliest to occur toward the end of an eddy’s life when the effects of eddy pumping and Ekman pumping are reduced (Huang et al., 2017). The change in chl-*a* concentration outside of the eddy is

$$\frac{dB_{out}}{dt} = \mu B_{out} + \Psi \left( \frac{A_{in}}{A_{out}} \right) (B_{in} - B_{out}). \quad (7)$$

Substituting Equations 1 and 7 into Equation 6,

$$\frac{d}{dt}(\delta c_{loc}) = \left( \mu - \frac{4}{3}\Psi \right) (B_{in} - B_{out}) \quad (8)$$

for a circular eddy ( $A_{in} = \pi r^2$ ). Equation 8 suggests that a larger  $\Psi$  (i.e., a leakier boundary) will cause elevated chl-*a* in an eddy to dilute more rapidly (Text S1). A positive  $\frac{d}{dt}(\delta c_{loc})$  is sustained when  $\mu > \frac{4\Psi}{3}$  and  $B_{in} > B_{out}$ . Since chl-*a* is anomalously high in Hawaiian Lee RCLVs, these features are most likely to meet both of these conditions, as exhibited in Figure 4. In most cases, however, an eddy-associated chl-*a* anomaly will decay via lateral dilution without sustained growth and low death rates.

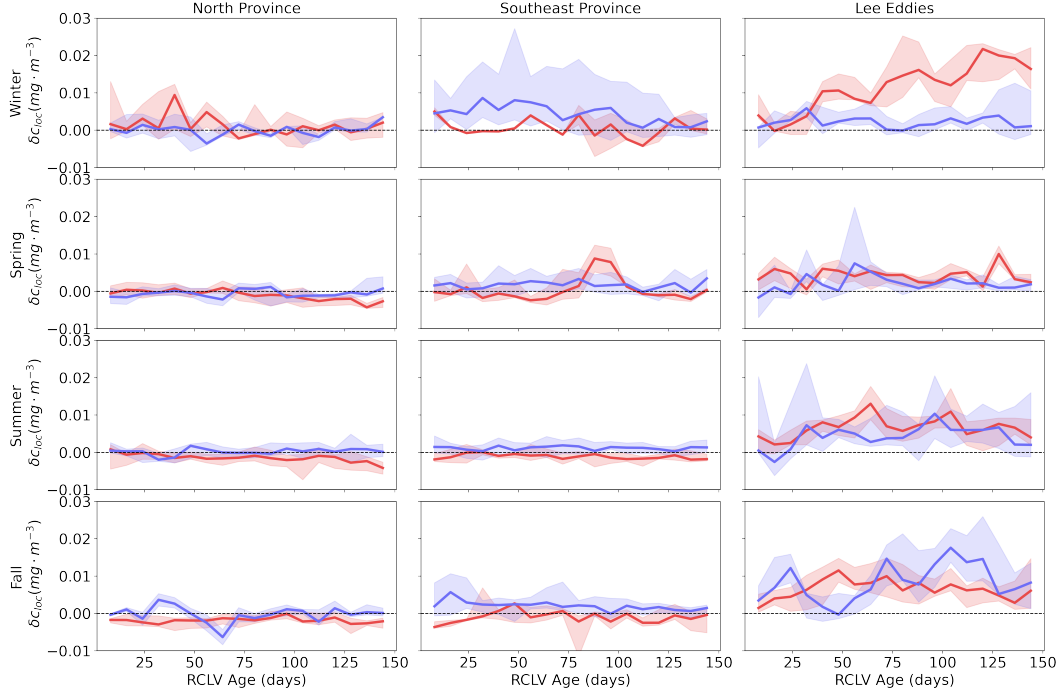


**Figure 4.** Local chl-*a* anomalies ( $\delta c_{loc}$ ) in RCLVs with lifespans of 150+ days. Each column corresponds to a mesoscale-driven province and each row with the season. Cyclonic (anticyclonic) eddies are in blue (red). The solid lines show the median  $\delta c_{loc}$  by RCLV age, and the shaded areas are the ranges of the 25% to 75% quantiles.

## 4 Discussion

Harnessing the temporal and spatial coverage of satellite observations, we measured the effects of mesoscale eddy trapping on chl-*a* concentrations in the NPSG. We compared Lagrangian (RCLV) and Eulerian (SLA) eddy atlases to distinguish signatures of chl-*a* in coherent eddies, dispersive eddies, and the background. Positive climatological chl-*a* anomalies are observed more in RCLVs than in SLA eddies or outside-eddy waters of the NPSG (Figure 1). However, trapping does not significantly shape the biological response to eddies everywhere. In northern latitudes ( $> 23^\circ\text{N}$ ), the chl-*a* signatures of coherent and leaky eddies are nearly indistinguishable (Figure 2). On the other hand, eddy trapping enhances chl-*a* signatures in the southeast ( $< 23^\circ\text{N}$ ) to varying amounts that depend on season and polarity. The response to coherency is strongest overall in the Hawaiian Lee eddies, where chl-*a* is enhanced year-round in RCLVs (Figure 3). The region and season also affect the slope of the chl-*a* anomaly as a function of the eddy age, which can be positive, negative, or constant (Figure 4).

Chl-*a* in the NPSG is more highly concentrated on average in anticyclonic RCLVs and SLA eddies than in cyclones and the background ocean (Table S1). In contrast, He et al. (2022) found anomalously high chlorophyll in Lagrangian coherent cyclones and low chlorophyll in anticyclones of the Northwest Pacific. Their results reflect particular biological signatures of warm and cold-core rings formed in the Kuroshio Current that translate into the gyre. Localized eddy features in the central gyre are far from such strong environmental gradients. In our study, we note that anticyclones are over-represented in the north (Table S2), the largest province within the domain, where they tend to elevate chl-*a*. Table S3 shows that cyclones are highly present in both the north and south-

east provinces, where chl-*a* anomalies in cyclones can be opposing. Our findings emphasize the complexity in the regional variations of the chl-*a* response to eddies of different polarities (Gaube et al., 2014). We also show definitive regional variations in the relationships of chl-*a* with eddy trapping.

A broad interpretation of the changes in chl-*a* at the mesoscale remains enigmatic. While Dufois et al. (2016) suggests that phytoplankton in subtropical gyre anticyclones are more productive in winter, others argue that changes in the chlorophyll-to-carbon ratio due to photoacclimation drive the signature (He et al., 2021). However, higher fish catch occurs in anticyclones compared to cyclones around the Hawaiian Islands (Arostegui et al., 2022), which may suggest that increased phytoplankton productivity supports higher trophic levels. Changes in chl-*a* may also indicate a change in community structure. Waga et al. (2019) used a size structure ocean color algorithm to infer that anticyclones in subtropical gyres support larger phytoplankton cells than cyclonic eddies. Eddy trapping may act to further alter community structure by separating populations and sheltering them from competition (Bracco et al., 2000). Interpreting whether the underlying phytoplankton communities differ in RCLVs and SLA eddies would require targeted in situ observations that could provide valuable insight into the observed relationships between eddies and chl-*a*.

Although satellites are the only ocean observing systems that obtain nearly full spatial coverage within days, a fundamental limitation is the restriction to the surface. The biological response to eddies at depth may differ from the surface signature (Huang & Xu, 2018; Zhao et al., 2021). Eddies affect subsurface chl-*a* in the NPSG by altering the depth of the deep chlorophyll maximum (Gaube et al., 2019; Xiu & Chai, 2020) and the vertical community structure (Olaizola et al., 1993; Brown et al., 2008; Fong et al., 2008; Barone et al., 2019). Here we focused on lateral biophysical interactions, but vertical mixing tied to the wind stress, heat exchange, and changes in the mixed layer depth will also influence the surface chl-*a* concentration (Gaube et al., 2013; McGillicuddy Jr, 2016). Moreover, the size of Lagrangian coherent boundaries may differ with depth (Nencioli et al., 2008; Ntaganou et al., 2023). Another limitation of satellite chl-*a* observations is missing data from cloud coverage including storms that can stimulate phytoplankton blooms in eddies (X. Liu et al., 2009; Shang et al., 2015; Villar et al., 2015; Chacko, 2017; Mikaelyan et al., 2020). Some of these limitations may be overcome by co-locating the bounds of RCLVs with autonomous vehicles and targeted shipboard observations of eddies, a promising avenue of future exploration.

Phytoplankton have a complex relationship with mesoscale eddy activity and respond depending on the polarity, trapping strength, location, season, and eddy age. By tracking Lagrangian coherent eddy boundaries from two decades of data in the NPSG, we show that eddy trapping can locally intensify chl-*a*. On the other hand, phytoplankton blooms generated inside SLA eddies may be quickly laterally advected and thus miss being associated with features once they leave the Eulerian bounds. It is important to consider dispersive eddy-associated perturbations since vertical mixing associated with submesoscale filaments stimulates primary production on eddy edges (Mahadevan, 2016; Guo et al., 2019) and lateral dilution of a chl-*a* patch can enhance the anomaly (Ser-Giacomi et al., 2023; Lehahn et al., 2017). We encourage future studies to employ Lagrangian metrics of coherency to support interpretations of biophysical interactions in eddies.

## Open Research Section

This study has been conducted using E.U. Copernicus Marine Service Information, namely the Level 4, 1/4° SLA and geostrophic velocity gridded global ocean dataset (Version 008\_047) distributed at <https://doi.org/10.48670/moi-00148>. 8-day average chl-*a* is produced by OC-CCI (Version 6.0 used here) and distributed by the European Space Agency at <https://www.oceancolour.org/> (Sathyendranath et al., 2019). The OceanEd-

dies MATLAB software that detects and tracks Eulerian SLA eddy contours is available at <https://github.com/ifrenger/OceanEddies> (Faghmous et al., 2015). The Ocean-Parcels v2.0 Python package used to run Lagrangian particle simulations is available at <https://oceanparcels.org/index.html> (Delandmeter & van Sebille, 2019). All figures were created with Matplotlib 3.3.4 (Caswell et al., 2021; Hunter, 2007), available under the Matplotlib license at <https://matplotlib.org/>.

The Python software developed for this study is available at <https://github.com/lexi-jones/RCLVatlas> (Jones-Kellett, 2023b). The code includes a pipeline to run Ocean-Parcels on Copernicus data, a custom kernel to calculate the relative vorticity along particle trajectories, and an RCLV tracking algorithm. The Jupyter notebook script [https://github.com/lexi-jones/RCLVatlas/blob/main/example\\_usage.ipynb](https://github.com/lexi-jones/RCLVatlas/blob/main/example_usage.ipynb) includes an example usage code for the software. The NPSG RCLV dataset is publicly available, distributed by Simons CMAP at [https://simonscmf.com/catalog/datasets/RCLV\\_atlas](https://simonscmf.com/catalog/datasets/RCLV_atlas) (Jones-Kellett, 2023a).

### Acknowledgments

We are grateful for support from the Simons Foundation (Simons Collaboration on Ocean Processes and Ecology, Award 329108, M.J.F.; CBIOMES, Award 549931, M.J.F.).

### Acronyms

**Chl-*a*** Chlorophyll-*a*  
**CMEMS** Copernicus Marine Service  
**LAVD** Lagrangian Averaged Vorticity Deviation  
**NPSG** North Pacific Subtropical Gyre  
**OC-CCI** Ocean Color Climate Change Initiative  
**PDD** Probability Density Distribution  
**RCLV** Rotationally Coherent Lagrangian Vortex  
**SLA** Sea Level Anomaly

### References

- Allen, C., Kanda, J., & Laws, E. (1996). New production and photosynthetic rates within and outside a cyclonic mesoscale eddy in the north pacific subtropical gyre. *Deep Sea Research Part I: Oceanographic Research Papers*, *43*, 917–936. doi: 10.1016/0967-0637(96)00022-2
- Arostegui, M., Gaube, P., Woodworth-Jefcoats, P., Kobayashi, D., & Braun, C. (2022). Anticyclonic eddies aggregate pelagic predators in a subtropical gyre. *Nature*, *609*, 535–540. doi: 10.1038/s41586-022-05162-6
- Barone, B., Coenen, A., Beckett, S., McGillicuddy, D., Jr., Weitz, J., & Karl, D. (2019). The ecological and biogeochemical state of the north pacific subtropical gyre is linked to sea surface height. *Journal of Marine Research*, *77*, 215–245. doi: 10.1357/002224019828474241
- Benitez-Nelson, C., Bidigare, R., Dickey, T., Landry, M., Leonard, C., Brown, S., ... Yang, E. (2007). Mesoscale eddies drive increased silica export in the subtropical pacific ocean. *Science*, *316*(5827), 1017–1021. doi: 10.1126/science.1136221
- Beron-Vera, F., Wang, Y., Olascoaga, M., Goni, G., & Haller, G. (2013). Objective detection of oceanic eddies and the agulhas leakage. *Journal of Physical Oceanography*, *43*, 1426–1438. doi: 10.1175/JPO-D-12-0171.1
- Bidigare, R., Benitez-Nelson, C., Leonard, C., Quay, P., Parsons, M., Foley, D., & Seki, M. (2003). Influence of a cyclonic eddy on microheterotroph biomass and

- carbon export in the lee of hawaii. *Geophysical Research Letters*, 30(6). doi: 10.1029/2002GL016393
- Bracco, A., Provenzale, A., & Scheuring, I. (2000). Mesoscale vortices and the paradox of the plankton. *Proceedings: Biological Sciences*, 267(1454), 1795–1800. doi: 10.1098/rspb.2000.1212
- Brown, S., Landry, M., Selph, K., Yang, E., Rii, Y., & Bidigare, R. (2008). Diatoms in the desert: Plankton community response to a mesoscale eddy in the subtropical north pacific. *Deep Sea Research Part II: Topical Studies in Oceanography*, 55, 1321–1333. doi: 10.1016/j.dsr2.2008.02.012
- Calil, P., & Richards, K. (2010). Transient upwelling hot spots in the oligotrophic north pacific. *Journal of Geophysical Research*, 115. doi: 10.1029/2009JC005360
- Calil, P., Richards, K., Jia, Y., & Bidigare, R. (2008). Eddy activity in the lee of the hawaiian islands. *Deep-Sea Research II*, 55, 1179–1194. doi: 10.1016/j.dsr2.2008.01.008
- Caswell, T., Droettboom, M., Lee, A., Sales de Andrade, E., Hunter, J., Firing, E., & et al. (2021). *Matplotlib v3.3.4* [Software]. Zenodo. Retrieved from <https://doi.org/10.5281/zenodo.4475376>
- Chacko, N. (2017). Chlorophyll bloom in response to tropical cyclone hudhud in the bay of bengal: Bio-argo subsurface observations. *Deep-Sea Research Part I*, 124, 66–72. doi: 10.1016/j.dsr.2017.04.010
- Chaigneau, A., Eldin, G., & Dewitte, B. (2009). Eddy activity in the four major upwelling systems from satellite altimetry (1992–2007). *Progress in Oceanography*, 83, 117–123. doi: 10.1016/j.pocean.2009.07.012
- Chelton, D., DeSzoeke, R., Schlax, M., El Naggar, K., & Siwertz, N. (1998). Geographic variability of the first baroclinic rossby radius of deformation. *Journal of Physical Oceanography*, 28, 433–460. doi: 10.1175/1520-0485(1998)028<0433:GVOTFB>2.0.CO;2
- Chelton, D., Gaube, P., Schlax, M., Early, J., & Samelson, R. (2011). The influence of nonlinear mesoscale eddies on near-surface oceanic chlorophyll. *Science*, 334, 328–332. doi: 10.1126/science.1208897
- Chelton, D., Schlax, M., & Samelson, R. (2011). Global observations of nonlinear mesoscale eddies. *Progress in Oceanography*, 91, 167–216. doi: 10.1016/j.pocean.2011.01.002
- Delandmeter, P., & van Sebille, E. (2019). The parcels v2.0 lagrangian framework: new field interpolation schemes. *Geoscientific Model Development*, 12, 3571–3584. doi: 10.5194/gmd-12-3571-2019
- d’Ovidio, F., De Monte, S., Della Penna, A., Cotte, C., & Guinet, C. (2013). Ecological implications of eddy retention in the open ocean: a lagrangian approach. *Journal of Physics A: Mathematical and Theoretical*, 46. doi: 10.1088/1751-8113/46/25/254023
- Dufois, F., Hardman-Mountford, N., Greenwood, J., Richardson, A., Feng, M., & Matear, R. (2016). Anticyclonic eddies are more productive than cyclonic eddies in subtropical gyres because of winter mixing. *Science Advances*, 2(5). doi: 10.1126/sciadv.1600282
- Faghmous, J., Frenger, I., Yao, Y., Warmka, R., Lindell, A., & Kumar, V. (2015). A daily global mesoscale ocean eddy dataset from satellite altimetry. *Scientific Data*, 2. doi: 10.1038/sdata.2015.28
- Falkowski, P., Ziemann, D., Kolber, Z., & Bienfang, P. (1991). Role of eddy pumping in enhancing primary production in the ocean. *Nature*, 352. doi: 10.1038/352055a0
- Fennel, K. (2001). The generation of phytoplankton patchiness by mesoscale current patterns. *Ocean Dynamics*, 52, 58–70. doi: 10.1007/s10236-001-0007-y5
- Fong, A., Karl, D., Lukas, R., Letelier, R., Zehr, J., & Church, M. (2008). Nitrogen fixation in an anticyclonic eddy in the oligotrophic north pacific ocean. *The*

- ISME Journal*, 2, 663–676. doi: 10.1038/ismej.2008.22
- Gaube, P., Chelton, D., Strutton, P., & Behrenfeld, M. (2013). Satellite observations of chlorophyll, phytoplankton biomass, and ekman pumping in nonlinear mesoscale eddies. *Journal of Geophysical Research: Oceans*, 118, 6349–6370. doi: 10.1002/2013JC009027
- Gaube, P., McGillicuddy Jr, D., Chelton, D., Behrenfeld, M., & Strutton, P. (2014). Regional variations in the influence of mesoscale eddies on near-surface chlorophyll. *Journal of Geophysical Research: Oceans*, 119, 8195–8220. doi: 10.1002/2014JC010111
- Gaube, P., McGillicuddy Jr., D., & Moulin, A. (2019). Mesoscale eddies modulate mixed layer depth globally. *Geophysical Research Letters*, 46, 1505–1512. doi: 10.1029/2018GL080006
- Geider, R. (1987). Light and temperature dependence of the carbon to chlorophyll a ratio in microalgae and cyanobacteria: implications for physiology and growth of phytoplankton. *New Phytologist*, 106, 1–34. doi: 10.1111/j.1469-8137.1987.tb04788.x
- Glover, D., Wroblewski, J. S., & McClain, C. (1994). Dynamics of the transition zone in coastal zone color scanner-sensed ocean color in the north pacific during oceanographic spring. *Journal of Geophysical Research: Oceans*, 99(C4), 7501–7511. doi: 10.1029/93JC02144
- Gower, J., Denman, K., & Holyer, R. (1980). Phytoplankton patchiness indicates the fluctuation spectrum of mesoscale oceanic structure. *Nature*, 288. doi: 10.1038/288157a0
- Guo, M., Xiu, P., Chai, F., & Xue, H. (2019). Mesoscale and submesoscale contributions to high sea surface chlorophyll in subtropical gyres. *Geophysical Research Letters*, 46(22), 13217–13226. doi: 10.1029/2019GL085278
- Haller, G. (2015). Lagrangian coherent structures. *Annual Review of Fluid Mechanics*, 47, 137–162. doi: 10.1146/annurev-fluid-010313-14132
- Haller, G., Hadjighasem, A., Farazmand, M., & Huhn, F. (2016). Defining coherent vortices objectively from the vorticity. *Journal of Fluid Mechanics*, 795, 136–173. doi: 10.1017/jfm.2016.151
- Harke, M., Frischkorn, K., Hennon, G., Haley, S., Barone, B., Karl, D., & Dyhrman, S. (2021). Microbial community transcriptional patterns vary in response to mesoscale forcing in the north pacific subtropical gyre. *Environmental Microbiology*, 23(8), 4807–4822. doi: 10.1111/1462-2920.15677
- He, Q., Tian, F., Yang, X., & Chen, G. (2022). Lagrangian eddies in the northwestern pacific ocean. *Journal of Oceanology and Limnology*, 40(1), 66–77. doi: 10.1007/s00343-021-0392-7
- He, Q., Zhan, H., Cai, S., & Zha, G. (2016). On the asymmetry of eddy-induced surface chlorophyll anomalies in the southeastern pacific: The role of eddy-ekman pumping. *Progress in Oceanography*, 141, 202–211. doi: 10.1016/j.pocean.2015.12.012
- He, Q., Zhan, H., Cai, S., & Zhan, W. (2021). Eddy-induced near-surface chlorophyll anomalies in the subtropical gyres: Biomass or physiology? *Geophysical Research Letters*, 48. doi: 10.1029/2020GL091975
- Huang, J., & Xu, F. (2018). Observational evidence of subsurface chlorophyll response to mesoscale eddies in the north pacific. *Global Biogeochemical Cycles*, 45, 8462–8470. doi: 10.1029/2018GL078408
- Huang, J., Xu, F., Zhou, K., Xiu, P., & Lin, Y. (2017). Temporal evolution of near-surface chlorophyll over cyclonic eddy lifecycles in the southeastern pacific. *Journal of Geophysical Research: Oceans*, 122, 6165–6179. doi: 10.1002/2017JC012915
- Hunter, J. D. (2007). Matplotlib: A 2d graphics environment. *Computing in Science & Engineering*, 9(3), 90–95. doi: 10.1109/MCSE.2007.55
- Jones-Kellett, A. (2023a). *North pacific subtropical gyre rclv atlas* [Dataset]. Zenodo.

- Retrieved from <https://doi.org/10.5281/zenodo.8139149>
- Jones-Kellett, A. (2023b). *Rclvatlas* [Software]. Zenodo. Retrieved from <https://doi.org/10.5281/zenodo.7702978>
- Jones-Kellett, A., & Follows, M. (*in review*, 2023). A lagrangian coherent eddy atlas for biogeochemical applications in the north pacific subtropical gyre. [preprint]. *Earth System Science Data Discussions*. doi: 10.5194/essd-2023-425
- Karl, D., & Church, M. (2017). Ecosystem structure and dynamics in the north pacific subtropical gyre: New views of an old ocean. *Ecosystems*, *20*, 433–457. doi: 10.1007/s10021-017-0117-0
- Lehahn, Y., d’Ovidio, F., & Koren, I. (2018). A satellite-based lagrangian view on phytoplankton dynamics. *Annual Review of Marine Science*, *10*, 99–119. doi: 10.1146/annurev-marine-121916-063204
- Lehahn, Y., d’Ovidio, F., Lévy, M., Amitai, Y., & Heifetz, E. (2011). Long range transport of a quasi isolated chlorophyll patch by an agulhas ring. *Geophysical Research Letters*, *38*. doi: 10.1029/2011GL048588
- Lehahn, Y., Koren, I., Sharoni, S., d’Ovidio, F., Vardi, A., & Boss, E. (2017). Dispersion/dilution enhances phytoplankton blooms in low-nutrient waters. *Nature Communications*, *8*(14868). doi: 10.1038/ncomms14868
- Liu, X., Wang, M., & Shi, W. (2009). A study of a hurricane katrina–induced phytoplankton bloom using satellite observations and model simulations. *Journal of Geophysical Research*, *114*. doi: 10.1029/2008JC004934
- Liu, Y., Dong, C., Guan, Y., Chen, D., McWilliams, J., & Nencioli, F. (2012). Eddy analysis in the subtropical zonal band of the north pacific ocean. *Deep-Sea Research I*, *68*, 54–67. doi: 10.1016/j.dsr.2012.06.001
- Lumpkin, C. (1998). *Eddies and currents of the hawaiian islands* (Unpublished doctoral dissertation). School of Ocean and Earth Science and Technology, University of Hawaii, Manoa.
- MacIntyre, H., Kana, T., & Geider, R. (2000). The effect of water motion on short-term rates of photosynthesis by marine phytoplankton. *Trends in Plant Science*, *5*(1), 12–17. doi: 10.1016/S1360-1385(99)01504-6
- Mahadevan, A. (2016). The impact of submesoscale physics on primary productivity of plankton. *Annual Review of Marine Science*, *8*, 161–184. doi: 10.1146/annurev-marine-010814-015912
- McGillicuddy Jr, D. (2016). Mechanisms of physical-biological-biogeochemical interaction at the oceanic mesoscale. *Annual Review of Marine Science*, *8*, 125–159. doi: 10.1146/annurev-marine-010814-015606
- Mikaelyan, A., Mosharov, S., Kubryakov, A., Pautova, L., Fedorov, A., & Chasovnikov, V. (2020). The impact of physical processes on taxonomic composition, distribution and growth of phytoplankton in the open black sea. *Journal of Marine Systems*, *208*. doi: 10.1016/j.jmarsys.2020.103368
- Nencioli, F., Kuwahara, V., Dickey, T., Rii, Y., & Bidigare, R. (2008). Physical dynamics and biological implications of a mesoscale eddy in the lee of hawai’i: Cyclone opal observations during e-flux iii. *Deep-Sea Research II*, *55*, 1252–1274. doi: 10.1016/j.dsr2.2008.02.003
- Nicholson, D., Emerson, S., & Eriksen, C. (2008). Net community production in the deep euphotic zone of the subtropical north pacific gyre from glider surveys. *Limnology and Oceanography*, *53*(5), 2226–2236. doi: 10.4319/lo.2008.53.5\_part\_2.2226
- Ntaganou, N., Kourafalou, V., Beron-Vera, F., Olascoaga, M., Le Hénaff, M., & Androulidakis, Y. (2023). Influence of caribbean eddies on the loop current system evolution. *Frontiers in Marine Science*, *10*. doi: 10.3389/fmars.2023.961058
- Olaizola, M., Ziemann, D., Bienfang, P., Walsh, W., & Conquest, L. (1993). Eddy-induced oscillations of the pycnocline affect the floristic composition and depth distribution of phytoplankton in the subtropical pacific. *Marine Biology*, *116*,

- 533-542. doi: 10.1007/BF00355471
- Provenzale, A. (1999). Transport by coherent barotropic vortices. *Annual Review of Fluid Mechanics*, *31*, 55-93. doi: 10.1146/annurev.fluid.31.1.55
- Rii, Y., Brown, S., Nencioli, F., Kuwahara, V., Dickey, T., Karl, D., & Bidigare, R. (2008). The transient oasis: Nutrient-phytoplankton dynamics and particle export in hawaiian lee cyclones. *Deep Sea Research Part II: Topical Studies in Oceanography*, *55*, 1275–1290. doi: 10.1016/j.dsr2.2008.01.013
- Sathyendranath, S., Brewin, R., Brockmann, C., Brotas, V., Calton, B., Chuprin, A., ... Platt, T. (2019). An ocean-colour time series for use in climate studies: the experience of the ocean-colour climate change initiative (oc-cci). *Sensors*, *19*(4285). doi: 10.3390/s19194285
- Ser-Giacomi, E., Martinez-Garcia, R., Dutkiewicz, S., & Follows, M. (2023). A lagrangian model for drifting ecosystems reveals heterogeneity-driven enhancement of marine plankton blooms. *Nature Communications*, *14*(6092). doi: 10.1038/s41467-023-41469-2
- Shang, X., Zhu, H., Chen, G., Xu, C., & Yang, Q. (2015). Research on cold core eddy change and phytoplankton bloom induced by typhoons: Case studies in the south china sea. *Advances in Meteorology*, *2015*. doi: 10.1155/2015/340432
- Tarshish, N., Abernathey, R., Zhang, C., Dufour, C., Frenger, I., & Griffies, S. (2018). Identifying lagrangian coherent vortices in a mesoscale ocean model. *Ocean Modelling*, *130*, 15–28. doi: 10.1016/j.ocemod.2018.07.001
- Travis, S., & Qiu, B. (2020). Seasonal reversal of the near-surface chlorophyll response to the presence of mesoscale eddies in the south pacific subtropical countercurrent. *Journal of Geophysical Research: Oceans*, *125*. doi: 10.1029/2019JC015752
- Vaillancourt, R., Marra, J., Seki, M., Parsons, M., & Bidigare, R. (2003). Impact of a cyclonic eddy on phytoplankton community structure and photosynthetic competency in the subtropical north pacific ocean. *Deep-Sea Research I*, *50*, 829–847. doi: 10.1016/S0967-0637(03)00059-1
- Villar, E., Farrant, G., Follows, M., Garczarek, L., Speich, S., Audic, S., ... Iudicone, D. (2015). Environmental characteristics of agulhas rings affect interocean plankton transport. *Science*, *348*(6237). doi: 10.1126/science.1261447
- Waga, H., Hirawake, T., & Ueno, H. (2019). Impacts of mesoscale eddies on phytoplankton size structure. *Geophysical Research Letters*, *46*(13), 191–198. doi: 10.1029/2019GL085150
- Wang, Y., Olascoaga, M., & Beron-Vera, F. (2015). Coherent water transport across the south atlantic. *Geophysical Research Letters*, *42*, 4072–4079. doi: 10.1002/2015GL064089
- Woods, J., & Onken, R. (1982). Diurnal variation and primary production in the ocean — preliminary results of a lagrangian ensemble model. *Journal of Plankton Research*, *4*(3). doi: 10.1093/plankt/4.3.735
- Xiu, P., & Chai, F. (2020). Eddies affect subsurface phytoplankton and oxygen distributions in the north pacific subtropical gyre. *Geophysical Research Letters*, *47*(15). doi: 10.1029/2020GL087037
- Xu, G., Dong, C., Liu, Y., Gaube, P., & Yang, J. (2019). Chlorophyll rings around ocean eddies in the north pacific. *Scientific Reports*, *9*. doi: 10.1038/s41598-018-38457-8
- Yoshida, S., Qiu, B., & Hacker, P. (2010). Wind-generated eddy characteristics in the lee of the island of hawaii. *Journal of Geophysical Research*, *115*. doi: 10.1029/2009JC005417
- Zhao, D., Xu, Y., Zhang, X., & Huang, C. (2021). Global chlorophyll distribution induced by mesoscale eddies. *Remote Sensing of Environment*, *254*. doi: 10.1016/j.rse.2020.112245
- Zhou, K., Benitez-Nelson, C., Huang, J., Xiu, P., Sun, Z., & Dai, M. (2021). Cy-

clonic eddies modulate temporal and spatial decoupling of particulate carbon, nitrogen, and biogenic silica export in the north pacific subtropical gyre. *Limnology and Oceanography*, 66(9). doi: 10.1002/lno.11895

# Lagrangian Eddy Trapping Fosters Chlorophyll Hot Spots in the North Pacific Subtropical Gyre

Alexandra E. Jones-Kellett<sup>1,2</sup>, Michael J. Follows<sup>1</sup>

<sup>1</sup>Department of Earth, Atmospheric, and Planetary Sciences, Massachusetts Institute of Technology,  
Cambridge, MA, USA

<sup>2</sup>Biology Department, Woods Hole Oceanographic Institution, Woods Hole, MA, USA

## Key Points:

- Cumulatively, Lagrangian coherent eddies have anomalously high surface chlorophyll relative to dispersive eddies and outside-eddy waters.
- The biological response to eddy trapping differs regionally, seasonally, by eddy age, and polarity.
- Coherent Hawaiian Lee eddies have the most extreme chlorophyll anomalies year-round relative to outside-eddy waters.

---

Corresponding author: Alexandra E. Jones-Kellett, [jonesae@mit.edu](mailto:jonesae@mit.edu)

**Abstract**

Vertical motions associated with mesoscale ocean eddies modulate the light and nutrient environment, stimulating anomalies in phytoplankton biomass and chlorophyll. Phytoplankton populations can be subsequently trapped by the horizontal circulation or laterally diluted. In a time-varying flow, Lagrangian methods can be used to quantify eddy trapping, also known as Lagrangian coherency. From two decades of remote sensing observations in the North Pacific Subtropical Gyre, we compared coincident Eulerian and Lagrangian eddy atlases to assess the impact of eddy trapping on chlorophyll concentration. We found higher chlorophyll within Lagrangian coherent boundaries than in Eulerian eddies and outside-eddy waters. Yet, there are differences regionally and seasonally. For example, chlorophyll is most enriched within coherent boundaries of the Hawaiian Lee eddies and to the south of 23°N in fall and winter. Our results suggest that by not accounting for lateral dilution, Eulerian analyses may underestimate the role of mesoscale eddies in enhancing chlorophyll.

**Plain Language Summary**

Eddies are ubiquitous rotating ocean currents up to hundreds of kilometers in diameter. While some eddies continuously mix with their surroundings, others trap their constituents that do not escape until the eddy dissolves. We refer to the former eddy behavior categorically as leaky or dispersive, while the latter is coherency. Phytoplankton are microscopic, free-floating microbes subject to the whims of ocean currents, including eddies. They contain the pigment chlorophyll within their cells that allows them to photosynthesize and subsequently alter the color of the ocean. In this study, we used satellite datasets and simulations of currents in the North Pacific to examine the effect of eddy coherency on local concentrations of phytoplankton, estimated by the greenness of the surface ocean. We found little difference in chlorophyll concentration in leaky and coherent eddies north of the Hawaiian Islands. To the south, we observed significantly greener waters in coherent eddies than in their leaky counterparts in the winter and fall. We suggest that, in some regions, studies may underestimate the role of leaky eddies in stimulating plankton blooms if they are quickly mixed with surrounding waters, which has implications for the ocean carbon budget.

**1 Introduction**

The North Pacific Subtropical Gyre (NPSG) has low phytoplankton biomass but is subject to high ecosystem variability (Karl & Church, 2017). Mesoscale eddies contribute to this variability, bringing nutrient-rich deep waters to the oligotrophic surface of the gyre via eddy-wind interactions and eddy pumping that stimulates phytoplankton growth (McGillicuddy Jr, 2016). Eddies in the NPSG including Station ALOHA and the Hawaiian Lee eddies are the focus of seminal works capturing biophysical interactions. For example, observations reveal that eddies affect biogeochemical cycling by enhancing primary production (Falkowski et al., 1991; Allen et al., 1996; Nicholson et al., 2008), altering phytoplankton community structure (Olaizola et al., 1993; Vaillancourt et al., 2003; Brown et al., 2008; Fong et al., 2008; Barone et al., 2019; Harke et al., 2021), and intensifying carbon export (Bidigare et al., 2003; Benitez-Nelson et al., 2007; Rii et al., 2008; Zhou et al., 2021). The NPSG is Earth’s largest ecosystem, thus the integrated effects of mesoscale biophysical interactions therein may play a significant role in the global carbon cycle.

Ocean eddies also influence the horizontal advection of phytoplankton, potentially acting to isolate communities (Provenzale, 1999) and preserve them across ocean basins (Lehahn et al., 2011; Villar et al., 2015). Further, lateral trapping can modulate trophic interactions (d’Ovidio et al., 2013) and generate plankton patchiness by localizing blooms (Gower et al., 1980; Fennel, 2001). In this study, we refer to eddies that trap for months

or longer as “coherent”. Mesoscale eddies that are detected from the Sea Level Anomaly (SLA) by assuming geostrophic balance (Chelton, Schlax, & Samelson, 2011; Chelton, Gaube, et al., 2011) are not necessarily coherent through time (Beron-Vera et al., 2013; Wang et al., 2015). To accurately measure eddy coherency in a time-varying flow, a Lagrangian perspective is needed (Haller, 2015). Interpreting biophysical interactions from a Lagrangian perspective naturally follows since phytoplankton experience a moving frame of reference (Woods & Onken, 1982; Lehahn et al., 2018).

Satellite remote sensing of SLA and chlorophyll-*a* (chl-*a*; a proxy for phytoplankton biomass) reveals significant relationships between ocean color anomalies and mesoscale eddies in subtropical waters (Gaube et al., 2014; Dufois et al., 2016; He et al., 2016; Huang et al., 2017; Xu et al., 2019; Travis & Qiu, 2020). However, these studies employ Eulerian methods and cannot determine the contribution of eddy trapping toward altering chl-*a* concentrations. By comparing complementary Lagrangian and Eulerian eddy atlases, we tested the hypothesis that the waters within coherent vortices more effectively maintain anomalous chl-*a* concentrations than leaky eddies (Figure S1). This is illustrated by the following idealized model that describes surface chl-*a* concentration in an eddy ( $B_{in}$ ):

$$\frac{dB_{in}}{dt} = \mu B_{in} - \Psi(B_{in} - B_{out}). \quad (1)$$

Here  $B_{out}$  is the outside-eddy concentration,  $\mu$  is the biological rate of change (e.g., growth, mortality, photoacclimation) in the eddy, and  $\Psi$  is the lateral fluid exchange rate at the eddy boundary. Chl-*a* concentrations increase inside an eddy when  $\mu B_{in} > \Psi(B_{in} - B_{out})$ . A coherent eddy minimizes  $\Psi$  over the timescale of interest. Thus,  $\frac{dB_{in}}{dt}$  will be greater in a coherent eddy than in a dispersive eddy with the same  $\mu$  and  $B_{out}$ , resulting in relatively higher chl-*a*. Our analysis of two decades of satellite data in the NPSG indeed reveals “hot spots” of chlorophyll (Calil & Richards, 2010) in Lagrangian coherent eddies and we uncover regional and seasonal differences in the biological signature of eddy trapping.

## 2 Materials and Methods

The domain includes 2000-2019 and the region 15-30°N, 180-230°. The spatial bounds reduce the degrees of freedom introduced by large-scale environmental variability from the ultra-oligotrophic western NPSG, Transition Zone Chlorophyll Front (Glover et al., 1994), California Current System, and equatorial currents (Figure S2). Moreover, focusing on a small area afforded a comprehensive evaluation of sub-regional and seasonal patterns. We used CMEMS 1/4° daily satellite geostrophic current and SLA data for eddy identification. 8-day average satellite chl-*a* data were obtained from OC-CCI with a spatial resolution of 4km at the equator (Sathyendranath et al., 2019).

### 2.1 Eddy Atlases

We used the OceanEddies software to generate an Eulerian eddy atlas from daily SLA (Faghmous et al., 2015). The algorithm identifies an eddy boundary as the outermost closed contour containing a single SLA extremum and tracks features through time. We required eddies to have a minimum lifetime of 32 days and contain at least twelve 1/4° grid cells. The smallest SLA eddy has an area of 8,048km<sup>2</sup> with a radius  $\approx 50$ km, consistent with the Rossby radius of deformation in the region of interest (Chelton et al., 1998). We set the eddy disappearance parameter to 3 days to account for noise in the data and prevent prematurely “killing” an eddy. We reduced the temporal resolution of the SLA atlas to an 8-day frequency for the ensuing analysis. In total, we tracked 6,846 SLA eddies (52,553 polygons), including 3,322 anticyclones characterized by SLA maxima and 3,524 cyclones by SLA minima.

Haller et al. (2016) introduced the Lagrangian Averaged Vorticity Deviation (LAVD), a measure of the integrated vorticity of a Lagrangian particle over a timescale of interest. An LAVD field is produced by mapping the LAVD for a grid of Lagrangian particles at their initialization locations. A fluid set in rigid-body rotation is identified as a closed contour surrounding a local maximum in the LAVD field, referred to as a Rotationally Coherent Lagrangian Vortex (RCLV) (Haller et al., 2016; Tarshish et al., 2018). Specifically tailored to biogeochemical applications, Jones-Kellett and Follows (*in review*, 2023) identified and tracked 32-day RCLVs in the NPSG at an 8-day resolution using backward-in-time particle simulations synchronized with the OC-CCI 8-day chl-*a* product (Figure S3). The atlas follows RCLVs from age 32 days and onward. Here, we expanded the dataset to capture RCLV genesis because young eddies are associated with biological anomalies (Gaube et al., 2013). To do so, we initialized Lagrangian particles in 32-day-old RCLVs and tracked them backward-in-time with the OceanParcels software (Delandmeter & van Sebille, 2019). At each 8-day “timestep” (ages 24, 16, and 8), we drew closed contours to encompass the particle set (Figure S4). The atlas contains 11,855 tracked RCLVs (75,445 polygons), including 5,592 anticyclones characterized by a negative sign of relative vorticity and 6,263 cyclones by a positive sign.

## 2.2 Chlorophyll Anomalies

We categorized each pixel from the satellite chl-*a* fields as background (i.e., outside-eddy) or inside an eddy. Some, though not all SLA eddies overlap with an RCLV, and vice versa. Thus, the in-eddy pixels are within an SLA eddy, RCLV, or both. We refer to the pixels inside an SLA eddy boundary but not an RCLV as “SLA excluding RCLV” (Figure S5). This includes the most dispersive regions of the eddy. The “SLA eddy” category includes all pixels within the eddy boundaries irrespective of whether it contains an RCLV.

The climatological chl-*a* anomaly is a temporal metric defined

$$\delta c_{clim}(x, y, t) = c(x, y, t) - \frac{1}{M} \sum_{t'=0}^M c(x, y, t') \quad (2)$$

where  $c(x, y, t)$  is the chl-*a* at location  $(x, y)$  and time  $t$ .  $\frac{1}{M} \sum_{t'=0}^M c(x, y, t')$  describes the 2000-2019 mean chl-*a* in the month corresponding to the date  $t$  (i.e., the monthly climatology; Figure S6). A positive  $\delta c_{clim}$  indicates that chl-*a* is higher than average for that location and month. We used  $\delta c_{clim}$  to identify changes in chl-*a* related to the mesoscale activity that were distinct from the seasonal cycle.

We define the relative difference in the eddy and background probability density distributions (PDD) of  $\delta c_{clim}$  as

$$f(\delta c_{clim}) = \frac{p_E(\delta c_{clim}) - p_B(\delta c_{clim})}{p_B(\delta c_{clim})} \quad (3)$$

where  $p_E(\delta c_{clim})$  is the PDD of the climatological chl-*a* anomalies in an eddy type and  $p_B(\delta c_{clim})$  is the PDD of anomalies in the background ocean.  $f(\delta c_{clim})$  is interpreted as the likelihood of observing a given chlorophyll anomaly in the eddy type compared to the background. For example,  $f(\delta c_{clim}) > 0$  means the value of  $\delta c_{clim}$  is more likely to be observed in an eddy than outside an eddy.

The local chl-*a* anomaly is a spatial metric defined

$$\delta c_{loc} = \frac{1}{A_{in}} \oint_I c(x, y) dI - \frac{1}{A_{out}} \oint_O c(x, y) dO. \quad (4)$$

$I$  is the eddy polygon with area  $A_{in}$  and  $O$  is the “donut” polygon from the eddy boundary to double the eddy radius with area  $A_{out}$ . Thus,  $\frac{1}{A_{in}} \oint_I c(x, y) dI$  is the average chl-*a* inside the eddy, and  $\frac{1}{A_{out}} \oint_O c(x, y) dO$  is the average in the immediate surroundings

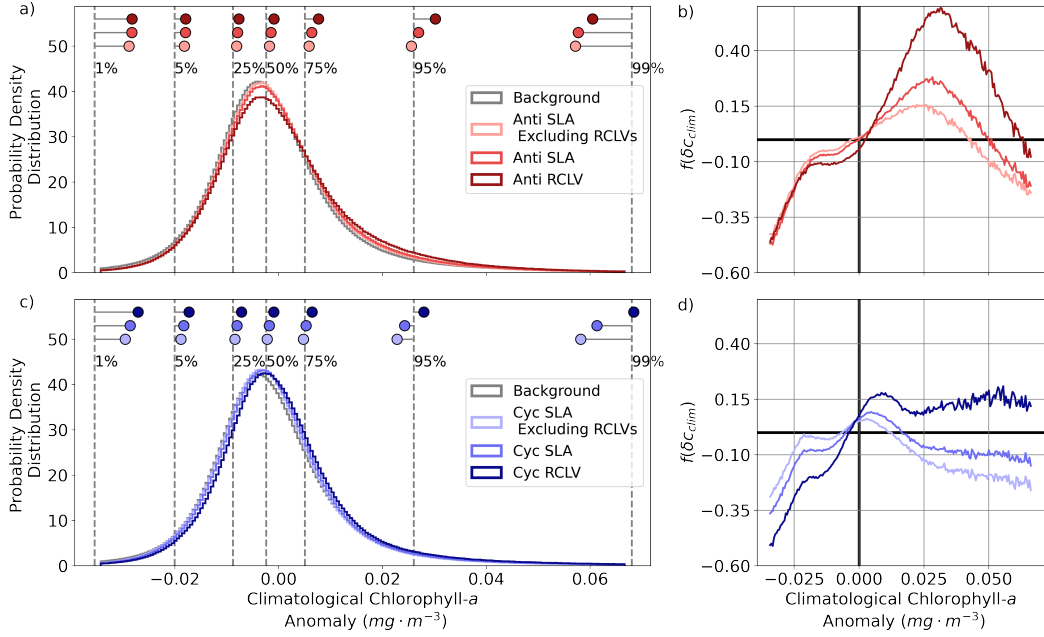


**Figure 1.** Probability density distributions (PDD) of the climatological chl-*a* anomalies ( $\delta c_{clim}$ ; Equation 2) in (a) anticyclones and (c) cyclones from the 1 – 99% quantiles. The dotted gray lines depict the quantiles of the background distribution, and the dots show the equivalent quantiles for each eddy category.  $f(\delta c_{clim})$  is the relative difference in the eddy PDD from the background PDD (Equation 3) for (b) anticyclones and (d) cyclones.

of the eddy. A positive  $\delta c_{loc}$  indicates that the mean chl-*a* concentration in the eddy is higher than surrounding waters.

### 3 Results

We address the hypothesis that coherent, isolated eddies will maintain anomalous chl-*a* longer than their dispersive counterparts. First, we address the cumulative impacts of eddy trapping. Next, we examine seasonal and sub-regional differences in the biological signature of eddy coherency.

#### 3.1 Cumulative Effect of Eddy Trapping

Cumulatively, surface chl-*a* is higher per unit area in RCLVs than in SLA eddies for both polarities (Table S1). On average, there is more surface chl-*a* in anticyclones than in the background and less in cyclones. Figure 1 shows the probability density distributions of the chl-*a* anomaly relative to the local, seasonal climatology ( $\delta c_{clim}$ ; Equation 2) for anticyclones (a) and cyclones (c). The quantiles of the distributions (indicated by the dots) show a consistent shift toward anomalously high chl-*a* in RCLVs (Figure 1a,c). An exception is the 99% quantile for anticyclones, which is lower than the background. This indicates that positive anomalies are more likely to occur in anticyclonic eddies than in the background ( $f > 0$ ; Equation 3) except at extremely high  $\delta c_{clim}$  (Figure 1b). Coherent cyclones have  $f > 0$  for all positive  $\delta c_{clim}$  (Figure 1d). Conversely, cyclonic SLA eddies have positive anomalies less frequently. 21% of chl-*a* in anticyclonic SLA eddies (Table S2) and 23% in cyclonic SLA eddies (Table S3) are also contained within an RCLV. We isolate the leakiest eddy zones when excluding RCLV-associated contri-

butions (“SLA excluding RCLVs” in Figure 1). Fewer positive chl-*a* anomalies are attributed to these zones in both polarities. Eddies are less likely than the background to have negative chl-*a* except for low-magnitude anomalies in cyclones.

### 3.2 Regional and Seasonal Subdomains

We examined the distributions of  $\delta c_{clim}$  seasonally and regionally to explore variations in how eddy trapping shapes chl-*a* in the NPSG. We determined mesoscale-driven subdomains by the eddy polarity probability ( $P$ ) (Chaigneau et al., 2009), defined

$$P(x, y) = \frac{F_A(x, y) - F_C(x, y)}{F_A(x, y) + F_C(x, y)}. \quad (5)$$

$F_A(x, y)$  ( $F_C(x, y)$ ) is the number of times the pixel at location  $(x, y)$  was inside an anticyclone (cyclone) from 2000-2019. Anticyclonic eddy polarity is more frequent than cyclonic when  $P > 0$ . Figure 2a depicts the geographic distribution of  $P$  for RCLVs, revealing more anticyclonic activity north of 23°N, cyclonic domination to the southeast of Hawai‘i, and Lee eddy signatures to the west.

There are distinctive chl-*a* signatures between northern and southeastern eddies (Figure 2). In the north, cyclones are less likely than the background to have positive  $\delta c_{clim}$  in all seasons except the summer. Northern cyclones are more likely to have a negative  $\delta c_{clim}$  than the background in winter and fall when domain-average chl-*a* concentrations are at the annual maximum (Figure S6, S7). According to Equation 1, a decrease in chl-*a* concentration ( $B_{in}$ ) may occur when  $\mu B_{in} < \Psi(B_{in} - B_{out})$ . In an RCLV where  $\Psi$  is minimized, it is likely that a low population growth rate,  $\mu$ , results in lower chl-*a*. For example, low nutrient supply rates may decrease growth rates, mortality may increase, or the cellular chlorophyll-to-carbon ratio can decrease due to increased light availability (Geider, 1987; MacIntyre et al., 2000). Northern anticyclones exhibit nearly opposite signatures than cyclones, with  $f > 0$  for positive  $\delta c_{clim}$  (except for extreme anomalies) in fall and winter. Anticyclonic RCLVs (and not SLA eddies) are likelier to have a negative chl-*a* anomaly relative to the summer and fall background. Leaky anticyclones uniquely have  $f > 0$  for highly positive  $\delta c_{clim}$  in the summer when mixing with surrounding chl-*a* elevated waters (high  $\Psi$  and high  $B_{out}$ ) may increase concentrations inside SLA anticyclones.

In the southeast province, the distributions of  $\delta c_{clim}$  in cyclones are inordinately different from that of the north. All types of cyclones have  $f < 0$  for negative  $\delta c_{clim}$  year-round, suggesting cyclones in this region enhance chl-*a*. In the fall and winter, cyclonic RCLVs are likelier to have a positive  $\delta c_{clim}$  than the background and SLA eddies. Because the chl-*a* signatures of cyclonic SLA eddies excluding RCLVs are like the background, positive anomalies in cyclonic SLA eddies are mostly contained within nested RCLVs. Thus, eddy trapping plays a significant role in the elevated chl-*a* in cyclones of the southeast province. Anticyclones in the southeast have  $f > 0$  for low magnitude positive  $\delta c_{clim}$  in the winter and spring. The distributions of  $\delta c_{clim}$  differ between RCLVs and SLA anticyclones during these seasons, suggesting that eddy trapping plays a distinctive role. Anticyclones are more likely than the background to host negative  $\delta c_{clim}$  in the fall. Anticyclones are less prevalent in the southeast province, so these observations play a small role in the cumulative effect in the gyre.

In summary, there are latitudinal biophysical differences within the NPSG. Anticyclones have high chl-*a* anomalies in the north during fall and winter and eddy trapping plays a minimal role in altering chl-*a* concentrations. In the southeast, cyclones foster high chl-*a* in fall and winter and chl-*a* is significantly higher in Lagrangian coherent vortices than in Eulerian eddies.

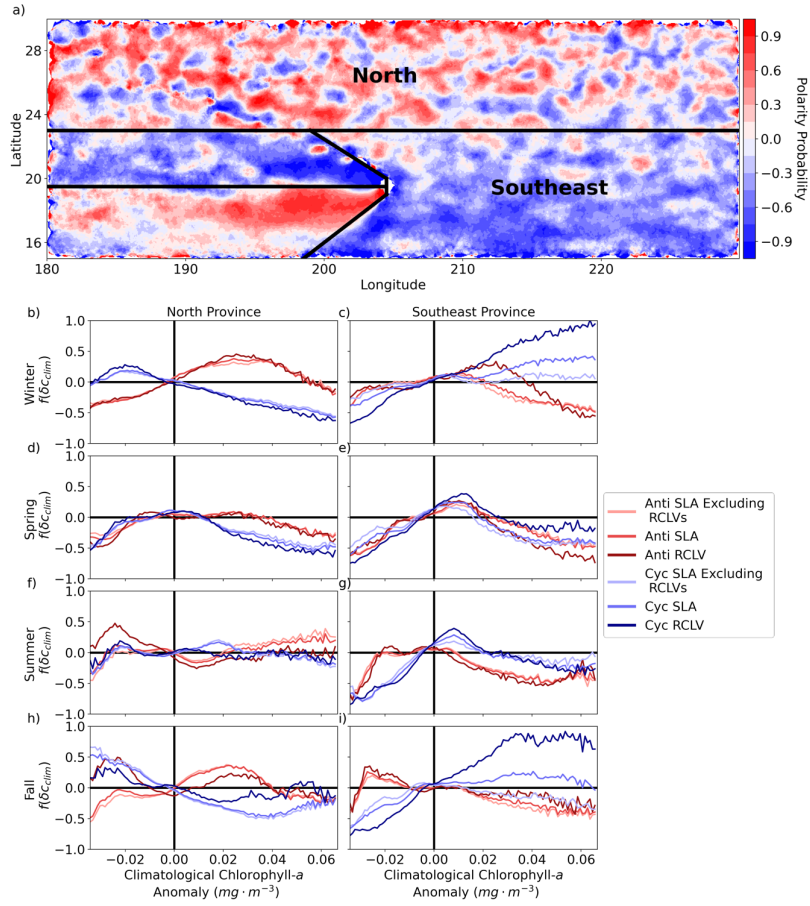


**Figure 2.** (a) RCLV polarity probability. Red (blue) indicates that anticyclones (cyclones) are more common at the location. The black lines delineate mesoscale-driven provinces. (b-i) The relative difference in the probability density distribution of the climatological chl-*a* anomaly from the background ( $f(\delta_{C_{lim}})$ ) for each eddy type. Each row corresponds with a season (winter includes December to February). Figures S8 and S9 show the underlying probability density distributions.

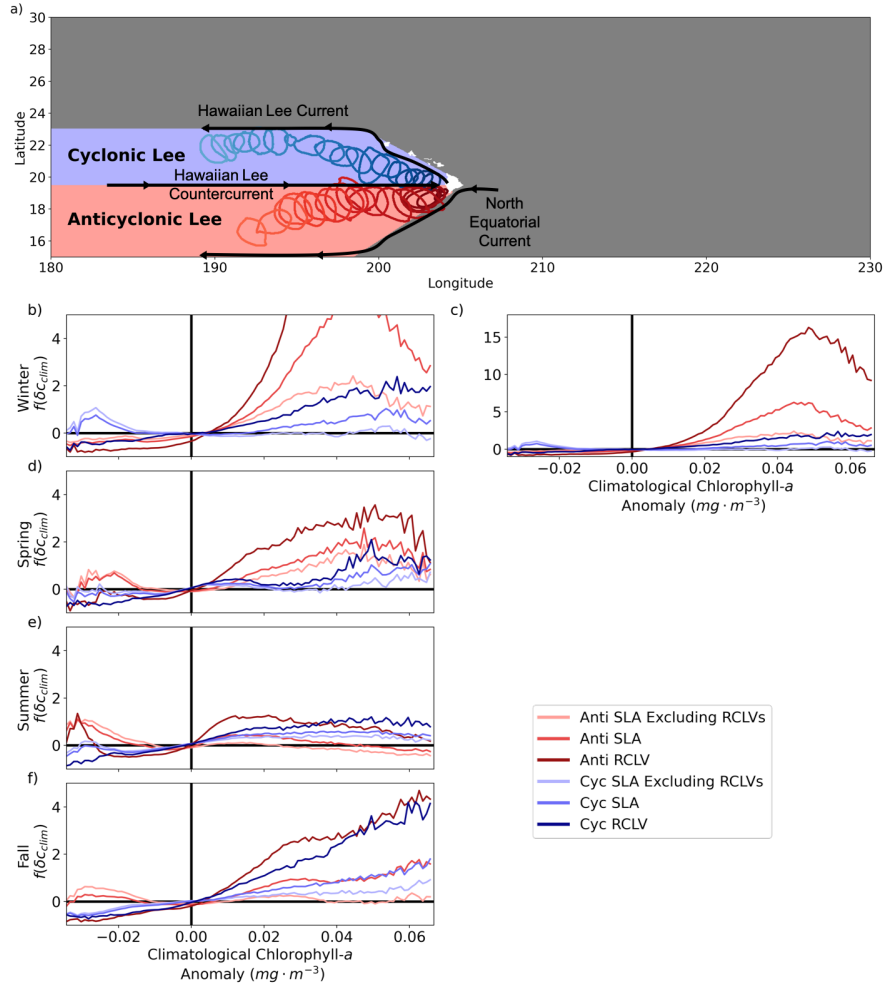


**Figure 3.** (a) Schematic of the currents that sustain the Hawaiian Lee eddies. The region dominated by cyclones (anticyclones) is blue (red). Two RCLV boundaries plotted every 16 days show the common propagation pathways westward from the islands. (b-f) The relative difference in probability density distributions of the climatological chl-*a* anomaly from the background ( $f(\delta c_{clim})$ ). Note that the y-axis differs from Figure 2 to accommodate larger values. Figure S10 depicts the underlying probability density distributions. Panel (c) includes the same information as (b) with a different y-axis to expose the curves.

### 3.3 Hawaiian Lee Eddies

The ‘‘Hawaiian Lee eddies’’ are large, long-lived features formed in the Lee of the Hawaiian Islands (Figure 3a). The shear instability between the eastward-flowing Hawaiian Lee Countercurrent and the westward-flowing North Equatorial Current generates anticyclones (Calil et al., 2008; Yoshida et al., 2010; Y. Liu et al., 2012). A wind stress curl anomaly associated with blocking trade winds by the islands produces cyclones (Lumpkin, 1998; Yoshida et al., 2010). The Hawaiian Lee Countercurrent to the south and the westward-flowing Hawaiian Lee Current to the north sustain the cyclonic vorticity.

RCLVs and SLA eddies of both polarities have  $f > 0$  for positive  $\delta c_{clim}$  year-round (Figure 3b-f). Trapping also plays a significant role in the chl-*a* signature of the Hawaiian Lee eddies. RCLVs have more positive chl-*a* anomalies than SLA eddies and the background ocean. We found a similar chl-*a* response to cyclonic and anticyclonic RCLVs in the summer and fall. However, anticyclones are more likely to have positive anomalies than cyclones in the winter and spring. Even the leakiest anticyclonic features (i.e., SLA excluding RCLVs) host positive  $\delta c_{clim}$  during these seasons. In the winter, anticyclonic RCLVs can be up to 15 times more likely than the background to have a positive  $\delta c_{clim}$ , whereas cyclonic RCLVs are up to 2 times as likely.

### 3.4 Chlorophyll Evolution of Long-lived Eddies

The Lagrangian eddy atlas enables the examination of chl-*a* patches as they evolve through time in quasi-isolated systems. Accordingly, we analyzed the in-eddy chl-*a* anomaly compared to the immediate surroundings,  $\delta c_{loc}$  (Equation 4), as a function of age for 245 RCLVs (109 anticyclones, 136 cyclones; Figure 4) that maintained coherency for 150 or more days. Figure S11 illustrates the westward propagation of these features. The magnitudes of  $\delta c_{loc}$  complement the results of Sections 3.2 and 3.3. For example, RCLVs in the north minimally alter chl-*a* compared to their surroundings except for wintertime anticyclones. In that case, the largest anomalies occur early in the lifetime. Cyclonic RCLVs foster heightened chl-*a* that declines with eddy age in the winter and fall in the southeast. Hawaiian Lee RCLVs dramatically localize chl-*a*, and this is the only domain where RCLVs have increasing  $\delta c_{loc}$  with eddy age. The results show that there is not a uniform slope of change in chl-*a* as a function of eddy age. Rather, chl-*a* evolves in coherent eddies depending on the region, season, and eddy polarity.

We apply the model of chl-*a* concentrations in eddies (Equation 1) to interpret the rate of change in  $\delta c_{loc}$  with RCLV age such that

$$\frac{d}{dt}(\delta c_{loc}) = \frac{dB_{in}}{dt} - \frac{dB_{out}}{dt}. \quad (6)$$

Consider the case where  $\mu$  is equivalent in and out of the eddy. This is likeliest to occur toward the end of an eddy’s life when the effects of eddy pumping and Ekman pumping are reduced (Huang et al., 2017). The change in chl-*a* concentration outside of the eddy is

$$\frac{dB_{out}}{dt} = \mu B_{out} + \Psi \left( \frac{A_{in}}{A_{out}} \right) (B_{in} - B_{out}). \quad (7)$$

Substituting Equations 1 and 7 into Equation 6,

$$\frac{d}{dt}(\delta c_{loc}) = \left( \mu - \frac{4}{3}\Psi \right) (B_{in} - B_{out}) \quad (8)$$

for a circular eddy ( $A_{in} = \pi r^2$ ). Equation 8 suggests that a larger  $\Psi$  (i.e., a leakier boundary) will cause elevated chl-*a* in an eddy to dilute more rapidly (Text S1). A positive  $\frac{d}{dt}(\delta c_{loc})$  is sustained when  $\mu > \frac{4\Psi}{3}$  and  $B_{in} > B_{out}$ . Since chl-*a* is anomalously high in Hawaiian Lee RCLVs, these features are most likely to meet both of these conditions, as exhibited in Figure 4. In most cases, however, an eddy-associated chl-*a* anomaly will decay via lateral dilution without sustained growth and low death rates.

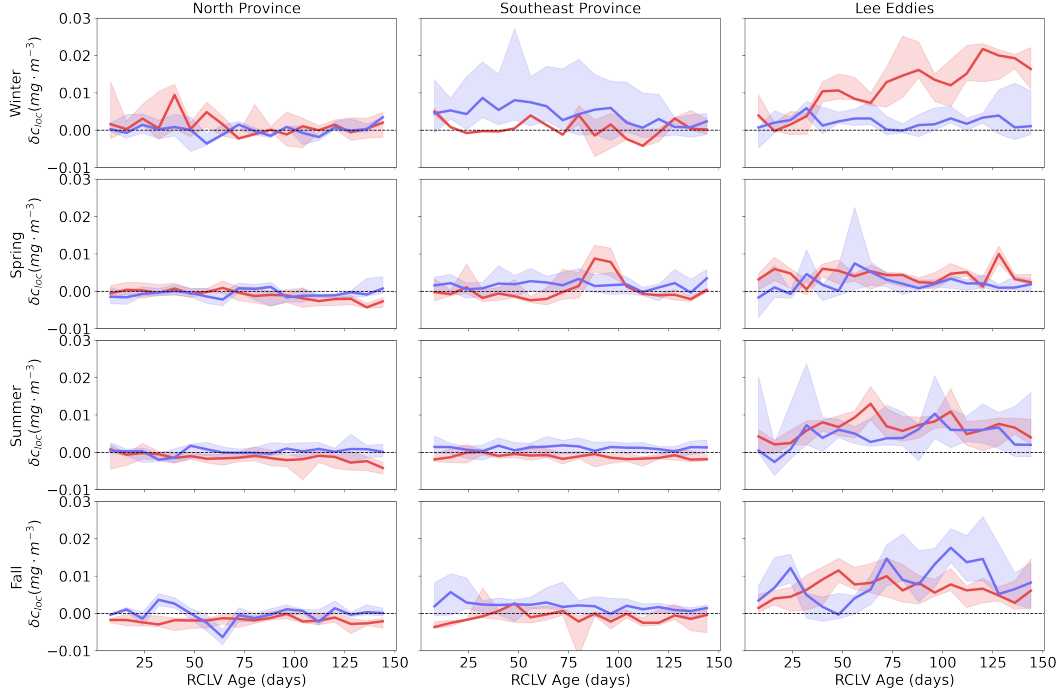


**Figure 4.** Local chl-*a* anomalies ( $\delta c_{loc}$ ) in RCLVs with lifespans of 150+ days. Each column corresponds to a mesoscale-driven province and each row with the season. Cyclonic (anticyclonic) eddies are in blue (red). The solid lines show the median  $\delta c_{loc}$  by RCLV age, and the shaded areas are the ranges of the 25% to 75% quantiles.

## 4 Discussion

Harnessing the temporal and spatial coverage of satellite observations, we measured the effects of mesoscale eddy trapping on chl-*a* concentrations in the NPSG. We compared Lagrangian (RCLV) and Eulerian (SLA) eddy atlases to distinguish signatures of chl-*a* in coherent eddies, dispersive eddies, and the background. Positive climatological chl-*a* anomalies are observed more in RCLVs than in SLA eddies or outside-eddy waters of the NPSG (Figure 1). However, trapping does not significantly shape the biological response to eddies everywhere. In northern latitudes ( $> 23^\circ\text{N}$ ), the chl-*a* signatures of coherent and leaky eddies are nearly indistinguishable (Figure 2). On the other hand, eddy trapping enhances chl-*a* signatures in the southeast ( $< 23^\circ\text{N}$ ) to varying amounts that depend on season and polarity. The response to coherency is strongest overall in the Hawaiian Lee eddies, where chl-*a* is enhanced year-round in RCLVs (Figure 3). The region and season also affect the slope of the chl-*a* anomaly as a function of the eddy age, which can be positive, negative, or constant (Figure 4).

Chl-*a* in the NPSG is more highly concentrated on average in anticyclonic RCLVs and SLA eddies than in cyclones and the background ocean (Table S1). In contrast, He et al. (2022) found anomalously high chlorophyll in Lagrangian coherent cyclones and low chlorophyll in anticyclones of the Northwest Pacific. Their results reflect particular biological signatures of warm and cold-core rings formed in the Kuroshio Current that translate into the gyre. Localized eddy features in the central gyre are far from such strong environmental gradients. In our study, we note that anticyclones are over-represented in the north (Table S2), the largest province within the domain, where they tend to elevate chl-*a*. Table S3 shows that cyclones are highly present in both the north and south-

east provinces, where chl-*a* anomalies in cyclones can be opposing. Our findings emphasize the complexity in the regional variations of the chl-*a* response to eddies of different polarities (Gaube et al., 2014). We also show definitive regional variations in the relationships of chl-*a* with eddy trapping.

A broad interpretation of the changes in chl-*a* at the mesoscale remains enigmatic. While Dufois et al. (2016) suggests that phytoplankton in subtropical gyre anticyclones are more productive in winter, others argue that changes in the chlorophyll-to-carbon ratio due to photoacclimation drive the signature (He et al., 2021). However, higher fish catch occurs in anticyclones compared to cyclones around the Hawaiian Islands (Arostegui et al., 2022), which may suggest that increased phytoplankton productivity supports higher trophic levels. Changes in chl-*a* may also indicate a change in community structure. Waga et al. (2019) used a size structure ocean color algorithm to infer that anticyclones in subtropical gyres support larger phytoplankton cells than cyclonic eddies. Eddy trapping may act to further alter community structure by separating populations and sheltering them from competition (Bracco et al., 2000). Interpreting whether the underlying phytoplankton communities differ in RCLVs and SLA eddies would require targeted in situ observations that could provide valuable insight into the observed relationships between eddies and chl-*a*.

Although satellites are the only ocean observing systems that obtain nearly full spatial coverage within days, a fundamental limitation is the restriction to the surface. The biological response to eddies at depth may differ from the surface signature (Huang & Xu, 2018; Zhao et al., 2021). Eddies affect subsurface chl-*a* in the NPSG by altering the depth of the deep chlorophyll maximum (Gaube et al., 2019; Xiu & Chai, 2020) and the vertical community structure (Olaizola et al., 1993; Brown et al., 2008; Fong et al., 2008; Barone et al., 2019). Here we focused on lateral biophysical interactions, but vertical mixing tied to the wind stress, heat exchange, and changes in the mixed layer depth will also influence the surface chl-*a* concentration (Gaube et al., 2013; McGillicuddy Jr, 2016). Moreover, the size of Lagrangian coherent boundaries may differ with depth (Nencioli et al., 2008; Ntaganou et al., 2023). Another limitation of satellite chl-*a* observations is missing data from cloud coverage including storms that can stimulate phytoplankton blooms in eddies (X. Liu et al., 2009; Shang et al., 2015; Villar et al., 2015; Chacko, 2017; Mikaelyan et al., 2020). Some of these limitations may be overcome by co-locating the bounds of RCLVs with autonomous vehicles and targeted shipboard observations of eddies, a promising avenue of future exploration.

Phytoplankton have a complex relationship with mesoscale eddy activity and respond depending on the polarity, trapping strength, location, season, and eddy age. By tracking Lagrangian coherent eddy boundaries from two decades of data in the NPSG, we show that eddy trapping can locally intensify chl-*a*. On the other hand, phytoplankton blooms generated inside SLA eddies may be quickly laterally advected and thus miss being associated with features once they leave the Eulerian bounds. It is important to consider dispersive eddy-associated perturbations since vertical mixing associated with submesoscale filaments stimulates primary production on eddy edges (Mahadevan, 2016; Guo et al., 2019) and lateral dilution of a chl-*a* patch can enhance the anomaly (Ser-Giacomi et al., 2023; Lehahn et al., 2017). We encourage future studies to employ Lagrangian metrics of coherency to support interpretations of biophysical interactions in eddies.

## Open Research Section

This study has been conducted using E.U. Copernicus Marine Service Information, namely the Level 4, 1/4° SLA and geostrophic velocity gridded global ocean dataset (Version 008\_047) distributed at <https://doi.org/10.48670/moi-00148>. 8-day average chl-*a* is produced by OC-CCI (Version 6.0 used here) and distributed by the European Space Agency at <https://www.oceancolour.org/> (Sathyendranath et al., 2019). The OceanEd-

dies MATLAB software that detects and tracks Eulerian SLA eddy contours is available at <https://github.com/ifrenger/OceanEddies> (Faghmous et al., 2015). The Ocean-Parcels v2.0 Python package used to run Lagrangian particle simulations is available at <https://oceanparcels.org/index.html> (Delandmeter & van Sebille, 2019). All figures were created with Matplotlib 3.3.4 (Caswell et al., 2021; Hunter, 2007), available under the Matplotlib license at <https://matplotlib.org/>.

The Python software developed for this study is available at <https://github.com/lexi-jones/RCLVatlas> (Jones-Kellett, 2023b). The code includes a pipeline to run Ocean-Parcels on Copernicus data, a custom kernel to calculate the relative vorticity along particle trajectories, and an RCLV tracking algorithm. The Jupyter notebook script [https://github.com/lexi-jones/RCLVatlas/blob/main/example\\_usage.ipynb](https://github.com/lexi-jones/RCLVatlas/blob/main/example_usage.ipynb) includes an example usage code for the software. The NPSG RCLV dataset is publicly available, distributed by Simons CMAP at [https://simonscmr.com/catalog/datasets/RCLV\\_atlas](https://simonscmr.com/catalog/datasets/RCLV_atlas) (Jones-Kellett, 2023a).

### Acknowledgments

We are grateful for support from the Simons Foundation (Simons Collaboration on Ocean Processes and Ecology, Award 329108, M.J.F.; CBIOMES, Award 549931, M.J.F.).

### Acronyms

**Chl-*a*** Chlorophyll-*a*  
**CMEMS** Copernicus Marine Service  
**LAVD** Lagrangian Averaged Vorticity Deviation  
**NPSG** North Pacific Subtropical Gyre  
**OC-CCI** Ocean Color Climate Change Initiative  
**PDD** Probability Density Distribution  
**RCLV** Rotationally Coherent Lagrangian Vortex  
**SLA** Sea Level Anomaly

### References

- Allen, C., Kanda, J., & Laws, E. (1996). New production and photosynthetic rates within and outside a cyclonic mesoscale eddy in the north pacific subtropical gyre. *Deep Sea Research Part I: Oceanographic Research Papers*, *43*, 917–936. doi: 10.1016/0967-0637(96)00022-2
- Arostegui, M., Gaube, P., Woodworth-Jefcoats, P., Kobayashi, D., & Braun, C. (2022). Anticyclonic eddies aggregate pelagic predators in a subtropical gyre. *Nature*, *609*, 535–540. doi: 10.1038/s41586-022-05162-6
- Barone, B., Coenen, A., Beckett, S., McGillicuddy, D., Jr., Weitz, J., & Karl, D. (2019). The ecological and biogeochemical state of the north pacific subtropical gyre is linked to sea surface height. *Journal of Marine Research*, *77*, 215–245. doi: 10.1357/002224019828474241
- Benitez-Nelson, C., Bidigare, R., Dickey, T., Landry, M., Leonard, C., Brown, S., ... Yang, E. (2007). Mesoscale eddies drive increased silica export in the subtropical pacific ocean. *Science*, *316*(5827), 1017–1021. doi: 10.1126/science.1136221
- Beron-Vera, F., Wang, Y., Olascoaga, M., Goni, G., & Haller, G. (2013). Objective detection of oceanic eddies and the agulhas leakage. *Journal of Physical Oceanography*, *43*, 1426–1438. doi: 10.1175/JPO-D-12-0171.1
- Bidigare, R., Benitez-Nelson, C., Leonard, C., Quay, P., Parsons, M., Foley, D., & Seki, M. (2003). Influence of a cyclonic eddy on microheterotroph biomass and

- carbon export in the lee of hawaii. *Geophysical Research Letters*, 30(6). doi: 10.1029/2002GL016393
- Bracco, A., Provenzale, A., & Scheuring, I. (2000). Mesoscale vortices and the paradox of the plankton. *Proceedings: Biological Sciences*, 267(1454), 1795–1800. doi: 10.1098/rspb.2000.1212
- Brown, S., Landry, M., Selph, K., Yang, E., Rii, Y., & Bidigare, R. (2008). Diatoms in the desert: Plankton community response to a mesoscale eddy in the subtropical north pacific. *Deep Sea Research Part II: Topical Studies in Oceanography*, 55, 1321–1333. doi: 10.1016/j.dsr2.2008.02.012
- Calil, P., & Richards, K. (2010). Transient upwelling hot spots in the oligotrophic north pacific. *Journal of Geophysical Research*, 115. doi: 10.1029/2009JC005360
- Calil, P., Richards, K., Jia, Y., & Bidigare, R. (2008). Eddy activity in the lee of the hawaiian islands. *Deep-Sea Research II*, 55, 1179–1194. doi: 10.1016/j.dsr2.2008.01.008
- Caswell, T., Droettboom, M., Lee, A., Sales de Andrade, E., Hunter, J., Firing, E., & et al. (2021). *Matplotlib v3.3.4* [Software]. Zenodo. Retrieved from <https://doi.org/10.5281/zenodo.4475376>
- Chacko, N. (2017). Chlorophyll bloom in response to tropical cyclone hudhud in the bay of bengal: Bio-argo subsurface observations. *Deep-Sea Research Part I*, 124, 66–72. doi: 10.1016/j.dsr.2017.04.010
- Chaigneau, A., Eldin, G., & Dewitte, B. (2009). Eddy activity in the four major upwelling systems from satellite altimetry (1992–2007). *Progress in Oceanography*, 83, 117–123. doi: 10.1016/j.pocean.2009.07.012
- Chelton, D., DeSzoeko, R., Schlax, M., El Naggar, K., & Siwertz, N. (1998). Geographic variability of the first baroclinic rossby radius of deformation. *Journal of Physical Oceanography*, 28, 433–460. doi: 10.1175/1520-0485(1998)028<0433:GVOTFB>2.0.CO;2
- Chelton, D., Gaube, P., Schlax, M., Early, J., & Samelson, R. (2011). The influence of nonlinear mesoscale eddies on near-surface oceanic chlorophyll. *Science*, 334, 328–332. doi: 10.1126/science.1208897
- Chelton, D., Schlax, M., & Samelson, R. (2011). Global observations of nonlinear mesoscale eddies. *Progress in Oceanography*, 91, 167–216. doi: 10.1016/j.pocean.2011.01.002
- Delandmeter, P., & van Sebille, E. (2019). The parcels v2.0 lagrangian framework: new field interpolation schemes. *Geoscientific Model Development*, 12, 3571–3584. doi: 10.5194/gmd-12-3571-2019
- d’Ovidio, F., De Monte, S., Della Penna, A., Cotte, C., & Guinet, C. (2013). Ecological implications of eddy retention in the open ocean: a lagrangian approach. *Journal of Physics A: Mathematical and Theoretical*, 46. doi: 10.1088/1751-8113/46/25/254023
- Dufois, F., Hardman-Mountford, N., Greenwood, J., Richardson, A., Feng, M., & Matear, R. (2016). Anticyclonic eddies are more productive than cyclonic eddies in subtropical gyres because of winter mixing. *Science Advances*, 2(5). doi: 10.1126/sciadv.1600282
- Faghmous, J., Frenger, I., Yao, Y., Warmka, R., Lindell, A., & Kumar, V. (2015). A daily global mesoscale ocean eddy dataset from satellite altimetry. *Scientific Data*, 2. doi: 10.1038/sdata.2015.28
- Falkowski, P., Ziemann, D., Kolber, Z., & Bienfang, P. (1991). Role of eddy pumping in enhancing primary production in the ocean. *Nature*, 352. doi: 10.1038/352055a0
- Fennel, K. (2001). The generation of phytoplankton patchiness by mesoscale current patterns. *Ocean Dynamics*, 52, 58–70. doi: 10.1007/s10236-001-0007-y5
- Fong, A., Karl, D., Lukas, R., Letelier, R., Zehr, J., & Church, M. (2008). Nitrogen fixation in an anticyclonic eddy in the oligotrophic north pacific ocean. *The*

- ISME Journal*, 2, 663–676. doi: 10.1038/ismej.2008.22
- Gaube, P., Chelton, D., Strutton, P., & Behrenfeld, M. (2013). Satellite observations of chlorophyll, phytoplankton biomass, and ekman pumping in nonlinear mesoscale eddies. *Journal of Geophysical Research: Oceans*, 118, 6349–6370. doi: 10.1002/2013JC009027
- Gaube, P., McGillicuddy Jr, D., Chelton, D., Behrenfeld, M., & Strutton, P. (2014). Regional variations in the influence of mesoscale eddies on near-surface chlorophyll. *Journal of Geophysical Research: Oceans*, 119, 8195–8220. doi: 10.1002/2014JC010111
- Gaube, P., McGillicuddy Jr., D., & Moulin, A. (2019). Mesoscale eddies modulate mixed layer depth globally. *Geophysical Research Letters*, 46, 1505–1512. doi: 10.1029/2018GL080006
- Geider, R. (1987). Light and temperature dependence of the carbon to chlorophyll a ratio in microalgae and cyanobacteria: implications for physiology and growth of phytoplankton. *New Phytologist*, 106, 1–34. doi: 10.1111/j.1469-8137.1987.tb04788.x
- Glover, D., Wroblewski, J. S., & McClain, C. (1994). Dynamics of the transition zone in coastal zone color scanner-sensed ocean color in the north pacific during oceanographic spring. *Journal of Geophysical Research: Oceans*, 99(C4), 7501–7511. doi: 10.1029/93JC02144
- Gower, J., Denman, K., & Holyer, R. (1980). Phytoplankton patchiness indicates the fluctuation spectrum of mesoscale oceanic structure. *Nature*, 288. doi: 10.1038/288157a0
- Guo, M., Xiu, P., Chai, F., & Xue, H. (2019). Mesoscale and submesoscale contributions to high sea surface chlorophyll in subtropical gyres. *Geophysical Research Letters*, 46(22), 13217–13226. doi: 10.1029/2019GL085278
- Haller, G. (2015). Lagrangian coherent structures. *Annual Review of Fluid Mechanics*, 47, 137–162. doi: 10.1146/annurev-fluid-010313-14132
- Haller, G., Hadjighasem, A., Farazmand, M., & Huhn, F. (2016). Defining coherent vortices objectively from the vorticity. *Journal of Fluid Mechanics*, 795, 136–173. doi: 10.1017/jfm.2016.151
- Harke, M., Frischkorn, K., Hennon, G., Haley, S., Barone, B., Karl, D., & Dyhrman, S. (2021). Microbial community transcriptional patterns vary in response to mesoscale forcing in the north pacific subtropical gyre. *Environmental Microbiology*, 23(8), 4807–4822. doi: 10.1111/1462-2920.15677
- He, Q., Tian, F., Yang, X., & Chen, G. (2022). Lagrangian eddies in the northwestern pacific ocean. *Journal of Oceanology and Limnology*, 40(1), 66–77. doi: 10.1007/s00343-021-0392-7
- He, Q., Zhan, H., Cai, S., & Zha, G. (2016). On the asymmetry of eddy-induced surface chlorophyll anomalies in the southeastern pacific: The role of eddy-ekman pumping. *Progress in Oceanography*, 141, 202–211. doi: 10.1016/j.pocean.2015.12.012
- He, Q., Zhan, H., Cai, S., & Zhan, W. (2021). Eddy-induced near-surface chlorophyll anomalies in the subtropical gyres: Biomass or physiology? *Geophysical Research Letters*, 48. doi: 10.1029/2020GL091975
- Huang, J., & Xu, F. (2018). Observational evidence of subsurface chlorophyll response to mesoscale eddies in the north pacific. *Global Biogeochemical Cycles*, 45, 8462–8470. doi: 10.1029/2018GL078408
- Huang, J., Xu, F., Zhou, K., Xiu, P., & Lin, Y. (2017). Temporal evolution of near-surface chlorophyll over cyclonic eddy lifecycles in the southeastern pacific. *Journal of Geophysical Research: Oceans*, 122, 6165–6179. doi: 10.1002/2017JC012915
- Hunter, J. D. (2007). Matplotlib: A 2d graphics environment. *Computing in Science & Engineering*, 9(3), 90–95. doi: 10.1109/MCSE.2007.55
- Jones-Kellett, A. (2023a). *North pacific subtropical gyre rclv atlas* [Dataset]. Zenodo.

- Retrieved from <https://doi.org/10.5281/zenodo.8139149>
- Jones-Kellett, A. (2023b). *Rclvatlas* [Software]. Zenodo. Retrieved from <https://doi.org/10.5281/zenodo.7702978>
- Jones-Kellett, A., & Follows, M. (*in review*, 2023). A lagrangian coherent eddy atlas for biogeochemical applications in the north pacific subtropical gyre. [preprint]. *Earth System Science Data Discussions*. doi: 10.5194/essd-2023-425
- Karl, D., & Church, M. (2017). Ecosystem structure and dynamics in the north pacific subtropical gyre: New views of an old ocean. *Ecosystems*, *20*, 433–457. doi: 10.1007/s10021-017-0117-0
- Lehahn, Y., d’Ovidio, F., & Koren, I. (2018). A satellite-based lagrangian view on phytoplankton dynamics. *Annual Review of Marine Science*, *10*, 99–119. doi: 10.1146/annurev-marine-121916-063204
- Lehahn, Y., d’Ovidio, F., Lévy, M., Amitai, Y., & Heifetz, E. (2011). Long range transport of a quasi isolated chlorophyll patch by an agulhas ring. *Geophysical Research Letters*, *38*. doi: 10.1029/2011GL048588
- Lehahn, Y., Koren, I., Sharoni, S., d’Ovidio, F., Vardi, A., & Boss, E. (2017). Dispersion/dilution enhances phytoplankton blooms in low-nutrient waters. *Nature Communications*, *8*(14868). doi: 10.1038/ncomms14868
- Liu, X., Wang, M., & Shi, W. (2009). A study of a hurricane katrina–induced phytoplankton bloom using satellite observations and model simulations. *Journal of Geophysical Research*, *114*. doi: 10.1029/2008JC004934
- Liu, Y., Dong, C., Guan, Y., Chen, D., McWilliams, J., & Nencioli, F. (2012). Eddy analysis in the subtropical zonal band of the north pacific ocean. *Deep-Sea Research I*, *68*, 54–67. doi: 10.1016/j.dsr.2012.06.001
- Lumpkin, C. (1998). *Eddies and currents of the hawaiian islands* (Unpublished doctoral dissertation). School of Ocean and Earth Science and Technology, University of Hawaii, Manoa.
- MacIntyre, H., Kana, T., & Geider, R. (2000). The effect of water motion on short-term rates of photosynthesis by marine phytoplankton. *Trends in Plant Science*, *5*(1), 12–17. doi: 10.1016/S1360-1385(99)01504-6
- Mahadevan, A. (2016). The impact of submesoscale physics on primary productivity of plankton. *Annual Review of Marine Science*, *8*, 161–184. doi: 10.1146/annurev-marine-010814-015912
- McGillicuddy Jr, D. (2016). Mechanisms of physical-biological-biogeochemical interaction at the oceanic mesoscale. *Annual Review of Marine Science*, *8*, 125–159. doi: 10.1146/annurev-marine-010814-015606
- Mikaelyan, A., Mosharov, S., Kubryakov, A., Pautova, L., Fedorov, A., & Chasovnikov, V. (2020). The impact of physical processes on taxonomic composition, distribution and growth of phytoplankton in the open black sea. *Journal of Marine Systems*, *208*. doi: 10.1016/j.jmarsys.2020.103368
- Nencioli, F., Kuwahara, V., Dickey, T., Rii, Y., & Bidigare, R. (2008). Physical dynamics and biological implications of a mesoscale eddy in the lee of hawai’i: Cyclone opal observations during e-flux iii. *Deep-Sea Research II*, *55*, 1252–1274. doi: 10.1016/j.dsr2.2008.02.003
- Nicholson, D., Emerson, S., & Eriksen, C. (2008). Net community production in the deep euphotic zone of the subtropical north pacific gyre from glider surveys. *Limnology and Oceanography*, *53*(5), 2226–2236. doi: 10.4319/lo.2008.53.5\_part\_2.2226
- Ntaganou, N., Kourafalou, V., Beron-Vera, F., Olascoaga, M., Le Hénaff, M., & Androulidakis, Y. (2023). Influence of caribbean eddies on the loop current system evolution. *Frontiers in Marine Science*, *10*. doi: 10.3389/fmars.2023.961058
- Olaizola, M., Ziemann, D., Bienfang, P., Walsh, W., & Conquest, L. (1993). Eddy-induced oscillations of the pycnocline affect the floristic composition and depth distribution of phytoplankton in the subtropical pacific. *Marine Biology*, *116*,

- 533-542. doi: 10.1007/BF00355471
- Provenzale, A. (1999). Transport by coherent barotropic vortices. *Annual Review of Fluid Mechanics*, *31*, 55-93. doi: 10.1146/annurev.fluid.31.1.55
- Rii, Y., Brown, S., Nencioli, F., Kuwahara, V., Dickey, T., Karl, D., & Bidigare, R. (2008). The transient oasis: Nutrient-phytoplankton dynamics and particle export in hawaiian lee cyclones. *Deep Sea Research Part II: Topical Studies in Oceanography*, *55*, 1275–1290. doi: 10.1016/j.dsr2.2008.01.013
- Sathyendranath, S., Brewin, R., Brockmann, C., Brotas, V., Calton, B., Chuprin, A., ... Platt, T. (2019). An ocean-colour time series for use in climate studies: the experience of the ocean-colour climate change initiative (oc-cci). *Sensors*, *19*(4285). doi: 10.3390/s19194285
- Ser-Giacomi, E., Martinez-Garcia, R., Dutkiewicz, S., & Follows, M. (2023). A lagrangian model for drifting ecosystems reveals heterogeneity-driven enhancement of marine plankton blooms. *Nature Communications*, *14*(6092). doi: 10.1038/s41467-023-41469-2
- Shang, X., Zhu, H., Chen, G., Xu, C., & Yang, Q. (2015). Research on cold core eddy change and phytoplankton bloom induced by typhoons: Case studies in the south china sea. *Advances in Meteorology*, *2015*. doi: 10.1155/2015/340432
- Tarshish, N., Abernathey, R., Zhang, C., Dufour, C., Frenger, I., & Griffies, S. (2018). Identifying lagrangian coherent vortices in a mesoscale ocean model. *Ocean Modelling*, *130*, 15–28. doi: 10.1016/j.ocemod.2018.07.001
- Travis, S., & Qiu, B. (2020). Seasonal reversal of the near-surface chlorophyll response to the presence of mesoscale eddies in the south pacific subtropical countercurrent. *Journal of Geophysical Research: Oceans*, *125*. doi: 10.1029/2019JC015752
- Vaillancourt, R., Marra, J., Seki, M., Parsons, M., & Bidigare, R. (2003). Impact of a cyclonic eddy on phytoplankton community structure and photosynthetic competency in the subtropical north pacific ocean. *Deep-Sea Research I*, *50*, 829–847. doi: 10.1016/S0967-0637(03)00059-1
- Villar, E., Farrant, G., Follows, M., Garczarek, L., Speich, S., Audic, S., ... Iudicone, D. (2015). Environmental characteristics of agulhas rings affect interocean plankton transport. *Science*, *348*(6237). doi: 10.1126/science.1261447
- Waga, H., Hirawake, T., & Ueno, H. (2019). Impacts of mesoscale eddies on phytoplankton size structure. *Geophysical Research Letters*, *46*(13), 191–198. doi: 10.1029/2019GL085150
- Wang, Y., Olascoaga, M., & Beron-Vera, F. (2015). Coherent water transport across the south atlantic. *Geophysical Research Letters*, *42*, 4072–4079. doi: 10.1002/2015GL064089
- Woods, J., & Onken, R. (1982). Diurnal variation and primary production in the ocean — preliminary results of a lagrangian ensemble model. *Journal of Plankton Research*, *4*(3). doi: 10.1093/plankt/4.3.735
- Xiu, P., & Chai, F. (2020). Eddies affect subsurface phytoplankton and oxygen distributions in the north pacific subtropical gyre. *Geophysical Research Letters*, *47*(15). doi: 10.1029/2020GL087037
- Xu, G., Dong, C., Liu, Y., Gaube, P., & Yang, J. (2019). Chlorophyll rings around ocean eddies in the north pacific. *Scientific Reports*, *9*. doi: 10.1038/s41598-018-38457-8
- Yoshida, S., Qiu, B., & Hacker, P. (2010). Wind-generated eddy characteristics in the lee of the island of hawaii. *Journal of Geophysical Research*, *115*. doi: 10.1029/2009JC005417
- Zhao, D., Xu, Y., Zhang, X., & Huang, C. (2021). Global chlorophyll distribution induced by mesoscale eddies. *Remote Sensing of Environment*, *254*. doi: 10.1016/j.rse.2020.112245
- Zhou, K., Benitez-Nelson, C., Huang, J., Xiu, P., Sun, Z., & Dai, M. (2021). Cy-

clonic eddies modulate temporal and spatial decoupling of particulate carbon, nitrogen, and biogenic silica export in the north pacific subtropical gyre. *Limnology and Oceanography*, 66(9). doi: 10.1002/lno.11895

# Supporting Information for “Lagrangian Eddy Trapping Fosters Chlorophyll Hot Spots in the North Pacific Subtropical Gyre”

DOI: 10.1002/

Alexandra E. Jones<sup>1,2</sup>, Michael J. Follows<sup>1</sup>

<sup>1</sup>Department of Earth, Atmospheric, and Planetary Sciences, Massachusetts Institute of Technology, Cambridge, MA, USA

<sup>2</sup>Biology Department, Woods Hole Oceanographic Institution, Woods Hole, MA, USA

## Contents of this file

1. Tables S1 to S3
2. Figures S1 to S12
3. Text S1

**Table S1.** Cumulative contributions to chl-*a* from 2000-2019 8-day averages<sup>a</sup>

	Chl- <i>a</i> ( $mg \cdot m^{-3}$ )	Fraction of Domain Chl- <i>a</i>	Area ( $km^2$ )	Fraction of Domain Area	$\frac{1}{\sum_i A_i} \sum_i Chl_i \cdot A_i$ ( $mg \cdot m^{-3}$ )
Domain	23,035,545	100%	6,790,256,191	100%	0.0671
Outside-eddy	19,083,498	82.880%	5,613,465,829	82.669%	0.0671
Anti RCLV	620,088	2.692%	181,066,346	2.667%	0.0678
Anti SLA	1,656,661	7.192%	487,216,799	7.175%	0.0672
Cyc RCLV	711,649	3.089%	214,517,840	3.159%	0.0661
Cyc SLA	1,711,740	7.431%	516,342,064	7.604%	0.0659

<sup>a</sup> Does not include area covered by clouds where chl-*a* is unknown.

**Table S2.** Number of pixels with available chl-*a* in each anticyclonic feature type.<sup>a</sup>

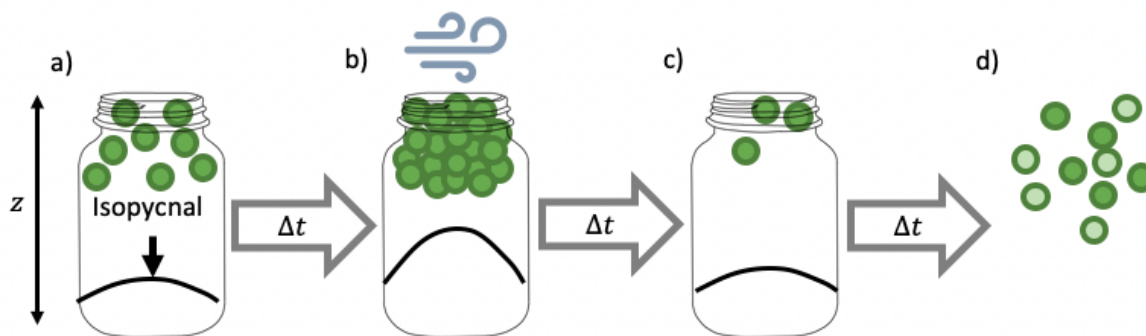
	Anti SLA	Anti RCLV	Anti SLA excluding RCLVs	% of Anti SLA data in RCLVs
Full Domain (all seasons)	24,611,335	9,145,426	19,472,926	20.88%
North Winter	2,573,257	888,074	2,154,500	16.27%
North Spring	2,989,498	1,233,772	2,297,869	23.14%
North Summer	3,537,936	1,482,487	2,675,426	24.38%
North Fall	3,035,172	1,059,554	2,498,944	17.67%
Southeast Winter	1,314,247	411,546	1,115,867	15.09%
Southeast Spring	1,374,094	456,698	1,120,926	18.42%
Southeast Summer	1,925,764	644,587	1,511,821	21.50%
Southeast Fall	1,658,451	544,226	1,356,411	18.21%
Lee Winter	1,599,300	639,110	1,218,971	23.78%
Lee Spring	1,347,659	522,509	1,055,755	21.66%
Lee Summer	1,648,147	636,421	1,249,902	24.16%
Lee Fall	1,607,810	626,442	1,216,534	24.34%

<sup>a</sup> Does not include area covered by clouds where chl-*a* is unknown.

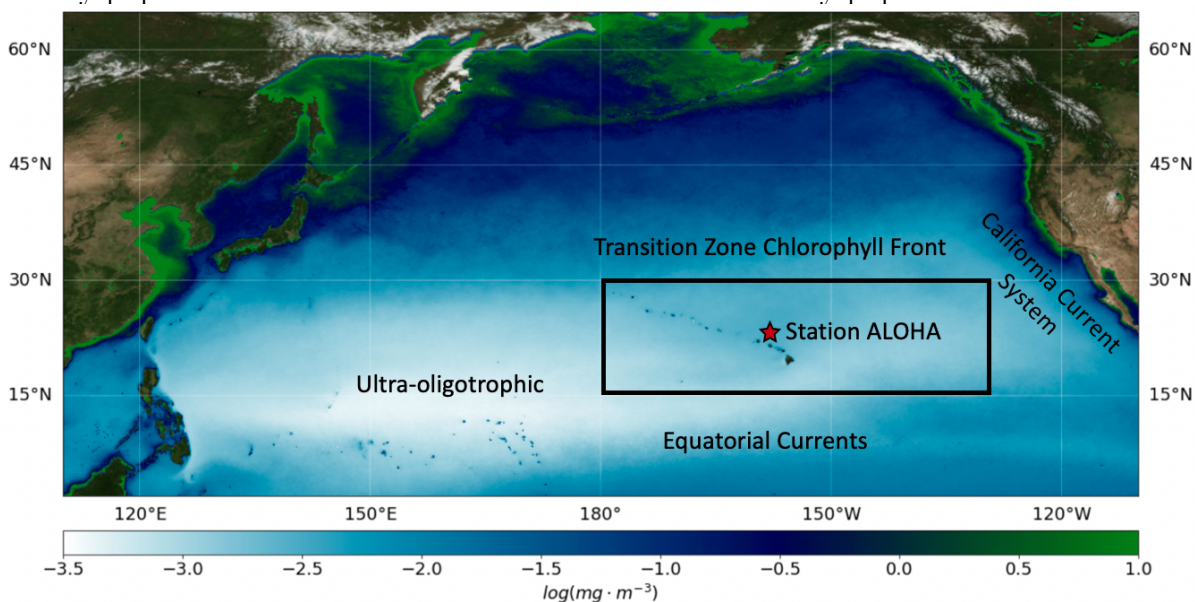
**Table S3.** Number of pixels with available chl-*a* in each cyclonic feature type.<sup>a</sup>

	Cyc SLA	Cyc RCLV	Cyc SLA excluding RCLVs	% of Cyc SLA data in RCLVs
Full Domain (all seasons)	25,960,826	10,758,238	19,943,322	23.18%
North Winter	2,369,956	784,780	2,015,018	14.98%
North Spring	2,438,519	1,036,121	1,986,213	18.55%
North Summer	3,257,596	1,247,902	2,604,223	20.06%
North Fall	2,678,662	895,421	2,263,668	15.49%
Southeast Winter	2,055,452	957,498	1,474,531	28.26%
Southeast Spring	2,072,384	977,892	1,434,013	30.80%
Southeast Summer	2,451,786	1,265,777	1,608,160	34.41%
Southeast Fall	2,057,854	1,046,325	1,441,224	29.96%
Lee Winter	1,383,511	519,921	1,105,519	20.09%
Lee Spring	1,607,596	709,743	1,185,369	26.26%
Lee Summer	1,981,864	772,515	1,499,457	24.34%
Lee Fall	1,605,646	544,343	1,325,927	17.42%

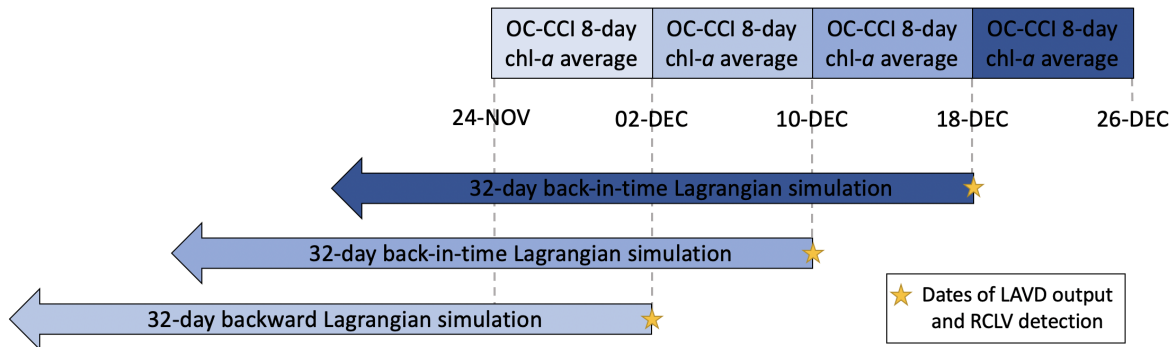
<sup>a</sup> Does not include area covered by clouds where chl-*a* is unknown.



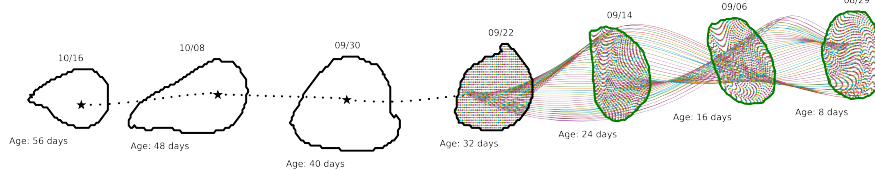
**Figure S1.** Schematic of the “hot spot” hypothesis. Here a jar is a metaphor for a perfect Rotationally Coherent Lagrangian Vortex (RCLV) where there is no exchange between the eddy and surrounding waters. **a)** The eddy spins up, and an initial phytoplankton population is trapped in the eddy. **b)** A phytoplankton bloom may occur in response to an environmental perturbation and is subsequently trapped and localized within the eddy bounds. **c)** A bloom decay or negative biological response would also be trapped in the vortex due to dilution limitation. **d)** When the eddy loses coherency, the in-eddy population mixes and interacts with the outside-eddy population.



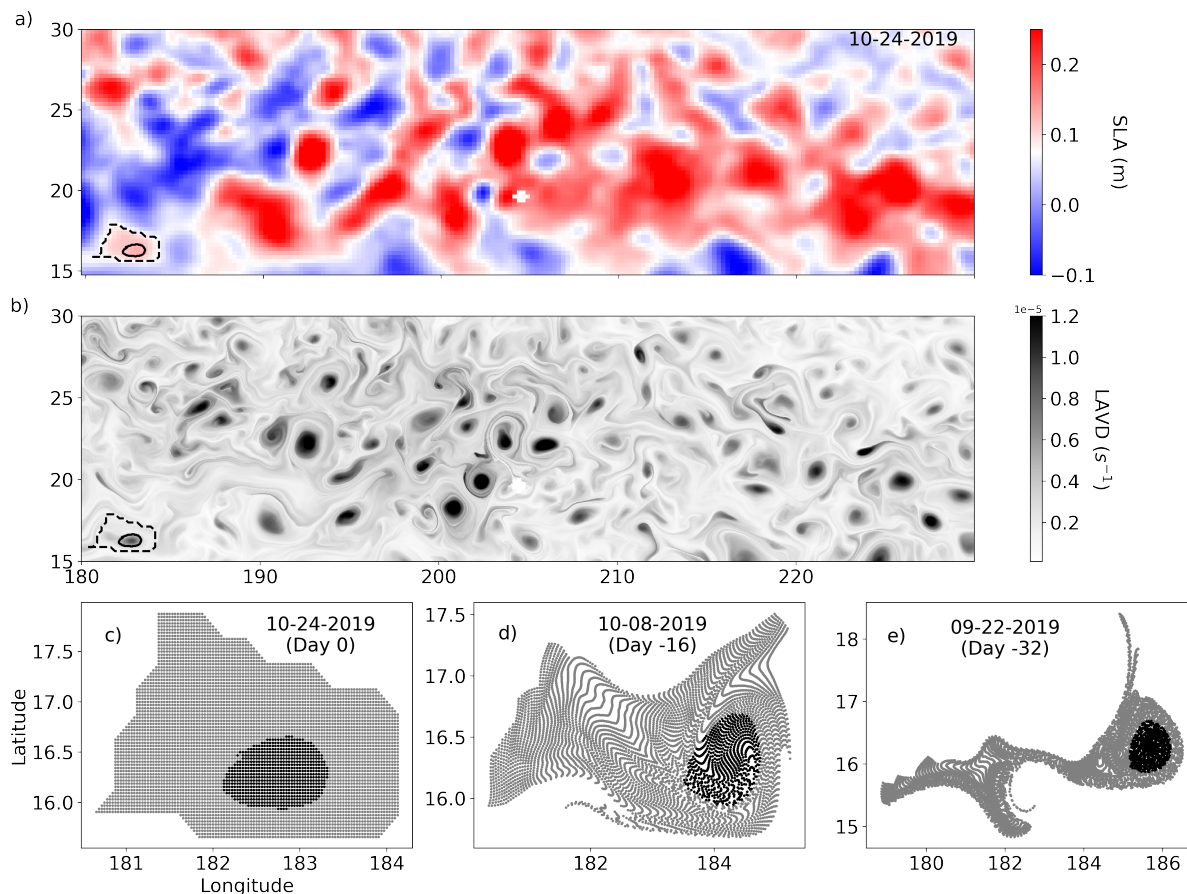
**Figure S2.** Average surface satellite chl-*a* from 2010-2020 in the North Pacific. The solid black box delineates the domain of this study.



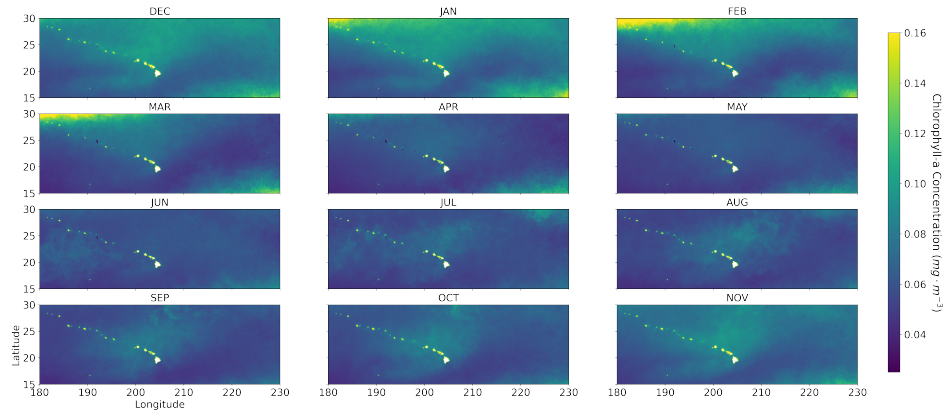
**Figure S3.** Temporal alignment between 32-day backward-in-time Lagrangian trajectories, RCLV detection, and the 8-day average OC-CCI observations. The blue colors match the RCLV detection dates and the collocated chlorophyll-a 8-day averages.



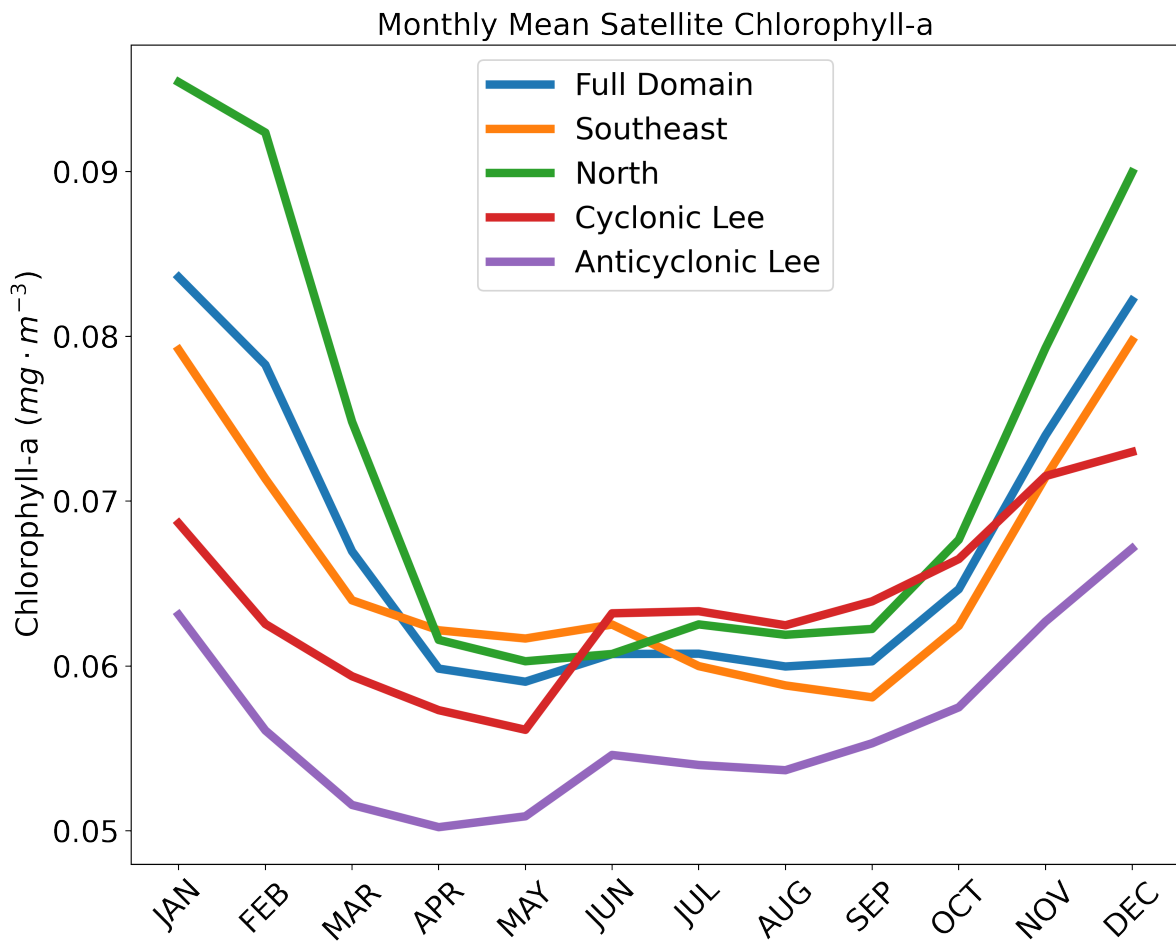
**Figure S4.** The [Jones-Kellett and Follows 2023] dataset tracked RCLVs forward in time starting with age 32 (date 09/22), shown in black. To simulate the RCLV genesis, we tracked Lagrangian particles contained with 32-day-old RCLVs backward-in-time. The green contours were drawn around the particle sets to represent the RCLV boundaries at ages 24 (09/14), 16 (09/06), and 8 days old (08/29).



**Figure S5.** An eddy on October 24th, 2019, with boundaries overlaid on the a) SLA and b) LAVD fields. The black dotted line represents the SLA eddy boundary, and the black solid line is the RCLV boundary. c) Initialization of the Lagrangian particles contained inside the SLA (gray and black) and RCLV (black) boundaries on October 24th, 2019. In this study, the gray particles are categorized as “SLA excluding RCLV”. d) The particle locations after advection 16 days backward-in-time and e) 32 days backward-in-time.

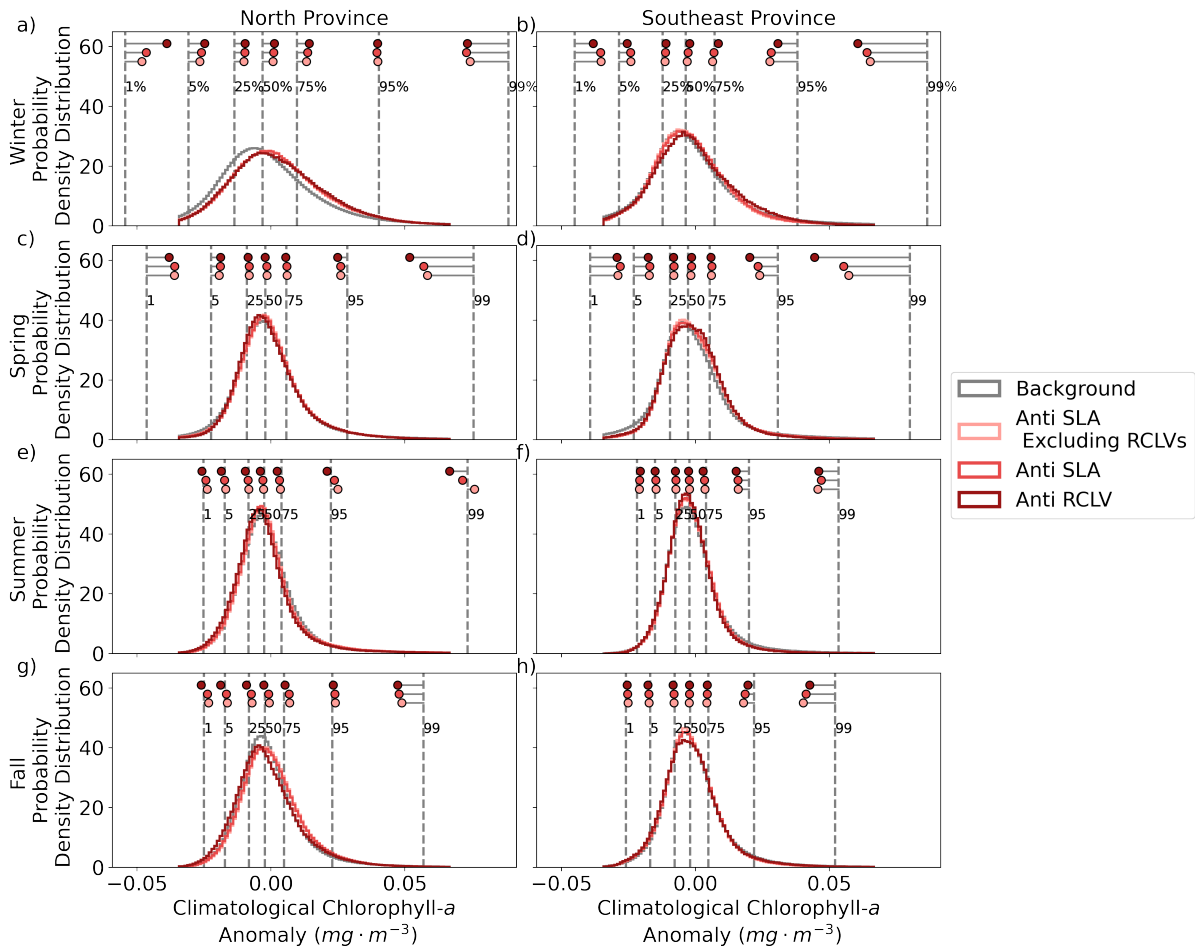


**Figure S6.** Monthly mean chl-*a* derived from 2000-2019 OC-CCI 8-day averages.



**Figure S7.** Monthly mean chl-*a* by province, calculated from 2000-2019 OC-CCI 8-day

averages.

**Figure S8.** Probability density distributions of the climatological chl-*a* anomaly for anticyclonic eddies in the north and southeast provinces. The vertical dotted gray lines depict the quantiles of the distribution of the background for that province and season, and the dots show the equivalent quantiles for each eddy category.

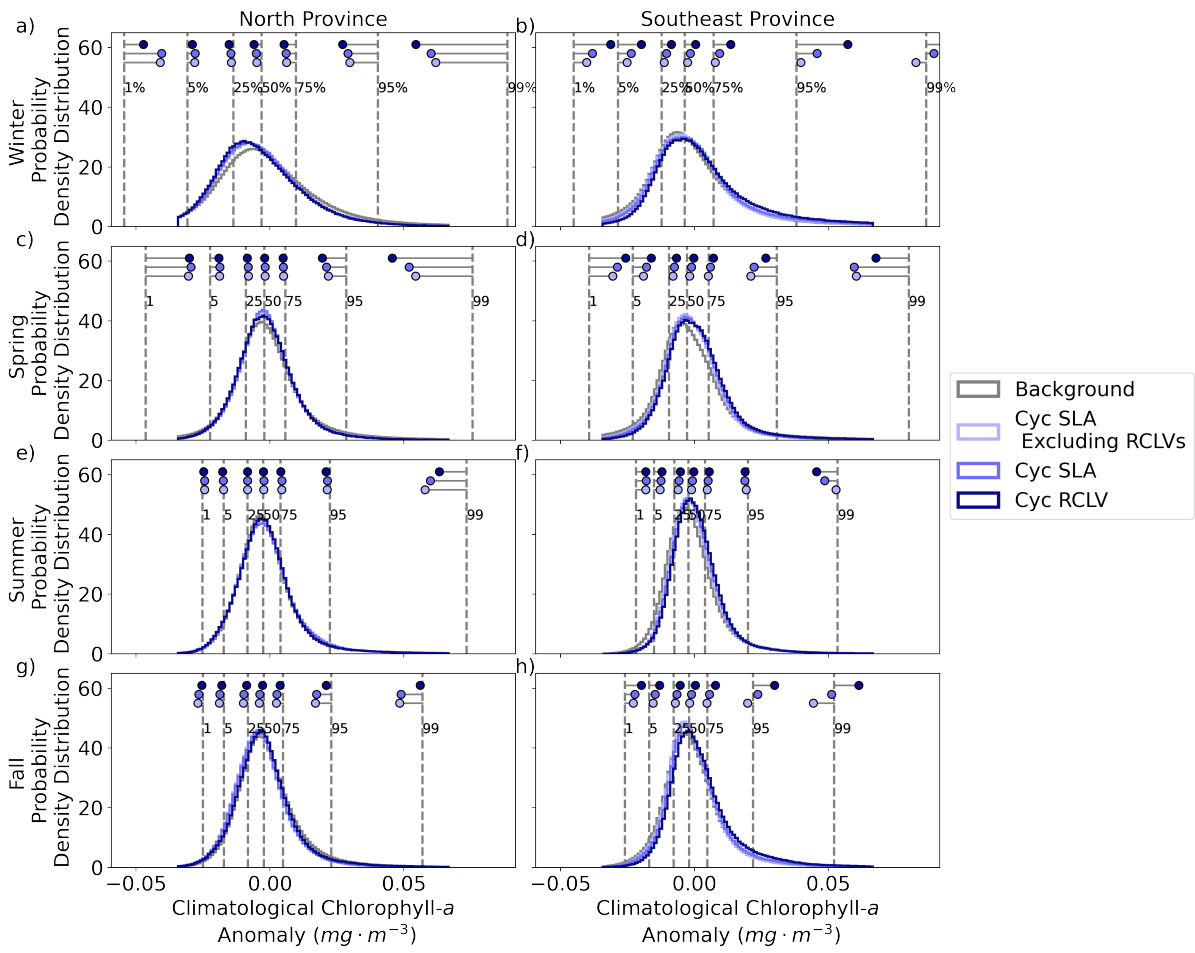


**Figure S9.** Same as Figure S8 but for cyclonic eddies.

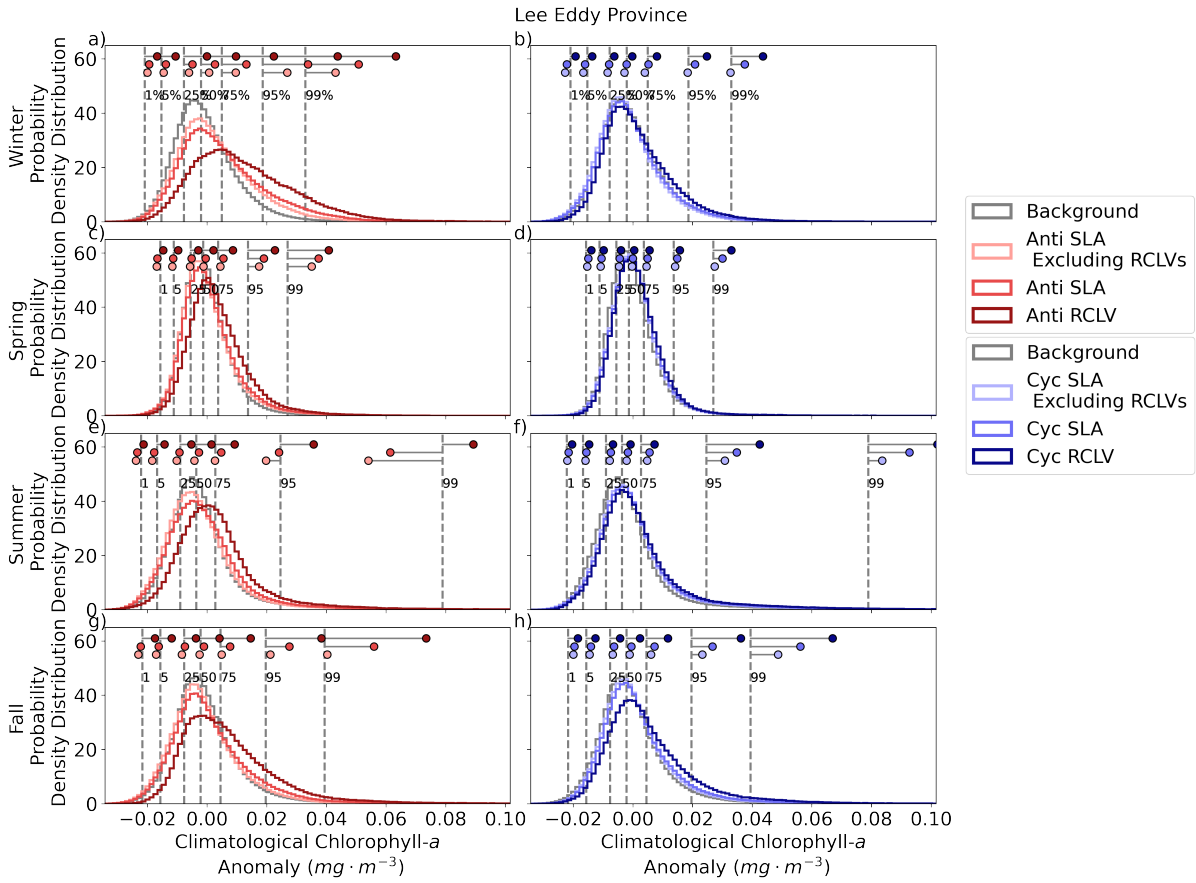


**Figure S10.** Same as Figure S8 and S9 but for the Hawaiian lee eddies.

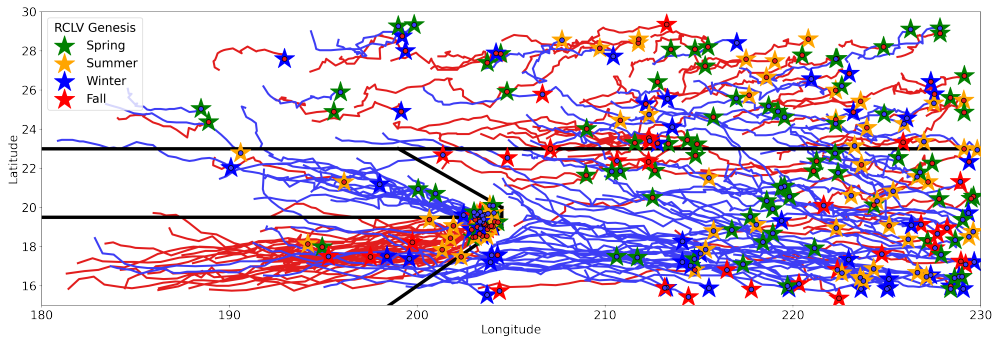


**Figure S11.** Trajectories of the eddy centers for long-lived (150+ day) RCLVs from 2000-2019. The cyclonic trajectories are in blue and the anticyclonic trajectories are in red. The dots and stars show the location of the eddy genesis, where the stars are color-coded by the birth season. The black lines show the boundaries of the mesoscale provinces used for the analysis in this study.

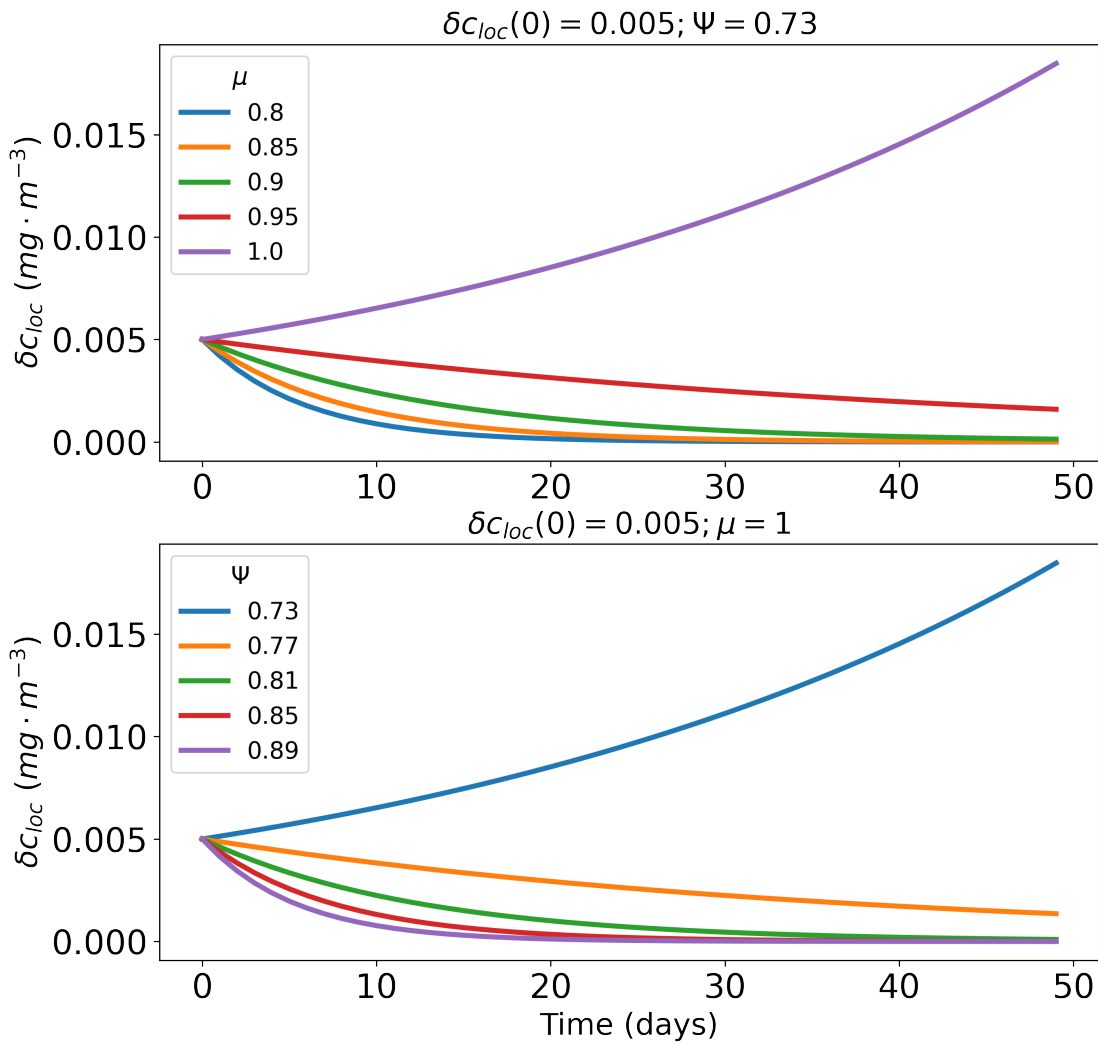


**Figure S12.** Solutions for Equation 8 of the main text. The top panel varies  $\mu$  while holding  $\Psi$  constant, and the bottom varies  $\Psi$  while holding  $\mu$  constant.

**Text S1.**

Equation 8 in the main text is a linear, 1st-order differential equation with the solution

$$\delta c_{loc}(t) = \delta c_{loc}(0)e^{(\mu_{in} - \frac{4}{3}\Psi)t} \quad (1)$$

where  $c_{loc}(0)$  is the initialization time. In Figure S12, we tested this model by holding the lateral exchange rate  $\Psi$  constant and varying the biological rate of change  $\mu$ , and vice versa. We find that both a high  $\mu$  and a low  $\Psi$  is needed in order to have an increase in  $c_{loc}$  with time.